

SACLANTCEN REPORT
serial no: SR-293

*SACLANT UNDERSEA
RESEARCH CENTRE
REPORT*



DETECTION OF BURIED OBJECTS
AT LOW GRAZING ANGLES:
PRELIMINARY EXPERIMENTAL RESULTS

W.L.J. Fox, A. Maguer

June 1998

The SACLANT Undersea Research Centre provides the Supreme Allied Commander Atlantic (SACLANT) with scientific and technical assistance under the terms of its NATO charter, which entered into force on 1 February 1963. Without prejudice to this main task – and under the policy direction of SACLANT – the Centre also renders scientific and technical assistance to the individual NATO nations.

This document is approved for public release.
Distribution is unlimited

SACLANT Undersea Research Centre
Viale San Bartolomeo 400
19138 San Bartolomeo (SP), Italy

tel: +39-0187-540.111
fax: +39-0187-524.600

e-mail: library@saclantc.nato.int

NORTH ATLANTIC TREATY ORGANIZATION

Detection of buried objects
at low grazing angles:
Preliminary experimental results

W. L. J. Fox and A. Maguer

The content of this document pertains to work performed under Project 031-1 of the SACLANTCEN Programme of Work. The document has been approved for release by The Director, SACLANTCEN.



Jan L. Spoelstra
Director

SACLANTCEN SR-293

intentionally blank page

SACLANTCEN SR-293

Detection of buried objects at
low grazing angles: Preliminary
experimental results

W. L. J. Fox and A. Maguer

Executive Summary:

Acoustic detection of objects buried in sandy ocean sediments has typically only been considered feasible using grazing angles above the *critical angle* of the sediment, where significant levels of sound can be transmitted into the sediment to scatter from buried targets. Below the critical angle, total internal reflection occurs. Although evanescent energy still exists in the sediment below the critical angle, its level falls off exponentially as a function of both depth into the sediment and frequency. Subcritical insonification geometries are desirable in order to increase coverage rate.

This report begins by reviewing simulation results showing the frequency dependence of buried target echo levels for subcritical insonification, and highlights the dominance of the lower frequency components. The frequency dependence of bottom backscatter is also discussed, showing a high dependence on the structure of the seabottom under consideration.

A recent experiment is then described in which backscatter measurements were made on buried objects both above and below the nominal critical angle. Preliminary processing of the data shows gains in signal-to-noise ratio can be obtained for subcritical grazing angles by emphasizing a relatively narrow band of frequencies at the lower end of the transmitted bandwidth, in empirical agreement with the reported model-based results. This is the first time, to the authors' knowledge, that this type of experimental data has been presented.

Future work in this area will focus on validation of models for buried target scattering and reverberation, leading to robust system designs that can reliably detect buried objects with high rates of coverage.

SACLANTCEN SR-293

intentionally blank page

SACLANTCEN SR-293

Detection of buried objects at
low grazing angles: Preliminary
experimental results

W. L. J. Fox and A. Maguer

Abstract:

This report considers the acoustic detection of objects buried in the seabed, and especially the possibility of using subcritical insonification geometries in order to increase coverage rate. Experimental results are presented for acoustic transmissions in the approximate frequency range 2–16 kHz both above and below the nominal critical angle of the sediment. The buried objects studied are a solid aluminum sphere of radius $a_s = 0.3$ m and a 2 m long water-filled cylindrical steel shell with radius $a_c = 0.25$ m. Preliminary processing of the data has shown that gains in signal-to-noise ratio can be obtained for subcritical cases by emphasizing the lower frequency components (in this case, $f < 3$ kHz) where models predict that the target echo is strongest due to the evanescent nature of the incident acoustic wave.

Keywords: detection ◦ buried ◦ subcritical

Contents

| | | |
|-----|---|----|
| 1 | Introduction | 1 |
| 2 | Theoretical and modeling background | 3 |
| 2.1 | Sound pressure levels in the seabottom | 3 |
| 2.2 | Scattering from buried targets | 5 |
| 2.3 | Bottom backscatter | 6 |
| 3 | Experiment description | 10 |
| 3.1 | Location and environment | 10 |
| 3.2 | Equipment | 10 |
| 3.3 | Targets | 13 |
| 3.4 | Geometry and equipment layout | 14 |
| 4 | Data analysis | 16 |
| 4.1 | Basic data description | 16 |
| 4.2 | Ping-to-ping fluctuations | 16 |
| 4.3 | Full band results | 22 |
| 4.4 | Low frequency processing and noise limitation | 27 |
| 4.5 | Low frequency results | 29 |
| 4.6 | Full band – low frequency comparison | 34 |
| 5 | Discussion | 36 |
| 6 | Acknowledgements | 38 |
| | References | 39 |

1

Introduction

Detection and classification of objects buried in ocean sediments is an important maritime research topic with many applications, including mine countermeasures. Man-made objects placed on the seabed can become buried due to a number of natural processes including impact and gravity sinking for softer sediments (e.g., muds and clays), and scouring, liquefaction, and bottom ripple migration for sandy seabeds [1].

In order to use acoustic methods to detect and classify buried targets, sound must be transmitted across the water-sediment interface, scatter from the target, and re-radiate into the water. If it is assumed for the moment that the water-sediment interface is a plane boundary separating two fluid half-spaces, the water has sound speed c_w , the sediment has sound speed c_s , and $c_s > c_w$, Snell's law predicts a so-called *critical grazing angle* [2], $\theta_c = \arccos(c_s/c_w)$. For grazing angles $\theta_g > \theta_c$, incident plane waves would produce a plane wave in the sediment with transmitted angle $\theta_t = \arccos((c_s/c_w) \cos \theta_g)$. For grazing angles below θ_c , the transmitted wave is *evanescent* and travels parallel to the interface, leading to the phenomenon called *total internal reflection*. The evanescent component in the sediment is an inhomogeneous wave. Its amplitude falls off exponentially with depth into the sediment and acoustic frequency [3]. As an example, a typical sound speed in sand is $c_s = 1650$ m/s [2] and in water is $c_w = 1500$ m/s, giving $\theta_c \approx 24.6^\circ$. Figure 1 shows a sketch of the various cases described here.

Previous work on buried object detection sonar systems has concentrated on supercritical insonification of the seabed. Here, transmission coefficients and Snell's Law ray paths can be calculated, and the limiting factor is the acoustic attenuation, which is usually assumed to be a linear function of frequency when expressed in dB/m [4], i.e., $\alpha = k_\alpha f$, where k_α depends on the sediment. Therefore, system design has depended on using frequencies below which the attenuation allows adequate echo level, and resolution considerations in order to reduce the size of the patch contributing to reverberation, hence maximizing the signal-to-noise ratio (SNR) for detection purposes.

By insonifying a larger part of the seafloor on a given ping, better coverage rates can be achieved. This would be possible by using subcritical insonification geometries. The problem is maintaining adequate signal-to-reverberation ratio for detec-

SACLANTCEN SR-293

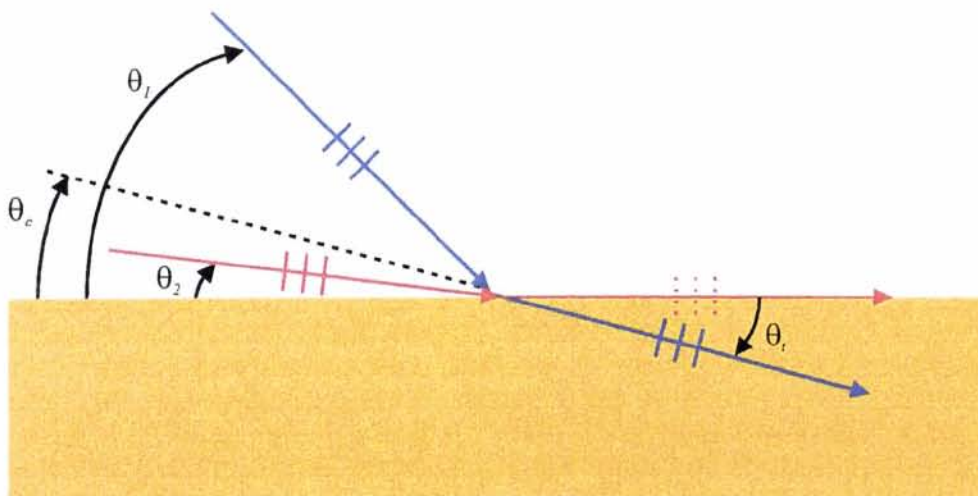


Figure 1 Sketch of supercritical ($\theta_g = \theta_1 > \theta_c$, blue) and subcritical ($\theta_g = \theta_2 < \theta_c$, red) insonification geometries (incident and transmitted waves are shown, reflected components are not). For θ_2 , the transmitted wave is evanescent, denoted by the dashed wave indicators.

tion given the relatively low levels of coherent energy arriving at the buried targets. Recent research efforts at SACLANTCEN have concentrated on this low grazing angle approach for frequencies below ~ 15 kHz using a parametric source as an experimental tool.

Section 2 of this report outlines previous work done on modeling of buried target echoes and reverberation. The dominance of the lower frequency components in monostatically measured buried target echoes at subcritical insonification will be highlighted. Section 3 describes a recent experiment for which buried target responses were measured over a large relative bandwidth of frequencies, and grazing angles both above and below the nominal critical angle. Section 4 displays some preliminary analysis of the data from this trial which shows empirical evidence for the ideas put forward in Sect. 2, i.e., that by concentrating on a narrow band of relatively lower frequencies where the evanescent field in the sediment and monostatic target echo levels still have relatively large amplitude, gains in SNR can be achieved over the wider band backscattered signals. Section 5 summarizes the results and outlines areas for future work.

SACLANTCEN SR-293

2

Theoretical and modeling background

As for any detection problem, high SNR is necessary for high probability of detection given an acceptably low probability of false alarm. The “signal” for the case under consideration is the echo returned from the buried object, and the “noise” will be a combination of ambient ocean noise and reverberation, most likely dominated by the effects of bottom backscatter.

In this section, some of the theoretical and modeling background for scattering from buried objects and bottom backscatter will be examined. The frequency dependence of these phenomena will be especially important. It should be noted that given certain assumptions (i.e., knowledge of the target echo, knowledge of the noise power spectral density, and Gaussian noise statistics), an optimal receiving filter can be designed [5, 6]. In this section, basic physical insights to the problem will be emphasized. Optimizing the source, transmit signal, receiver, etc., will be a topic of future efforts.

Since the primary application of our research has been in the field of mine countermeasures, targets with representative dimension $a \sim 0.25$ m will be considered. For the canonical shapes of spheres and cylinders, a is usually considered to be the radius. Sandy seabeds will also be mainly considered, where high coverage rate buried object detection is generally considered very difficult due to critical grazing angles which can be as high as $\sim 35^\circ$. It is convenient to keep in mind that ka is on the order of the acoustic frequency in kHz for these conditions.

This section is not intended as an exhaustive topic review, but gives inroads to the literature by citing a few of the most recent and pertinent publications in the areas of buried target scattering and seabed reverberation. The cited references themselves usually contain more extensive bibliographies for the interested reader.

2.1 *Sound pressure levels in the seabottom*

Before reviewing work on scattering from buried targets, it is instructive to examine sound pressure levels (SPL's) in the seabottom due to subcritical insonification in the context of the frequency range and nominal seabed conditions considered in this work. As mentioned in Sect. 1, subcritical insonification produces an evanescent

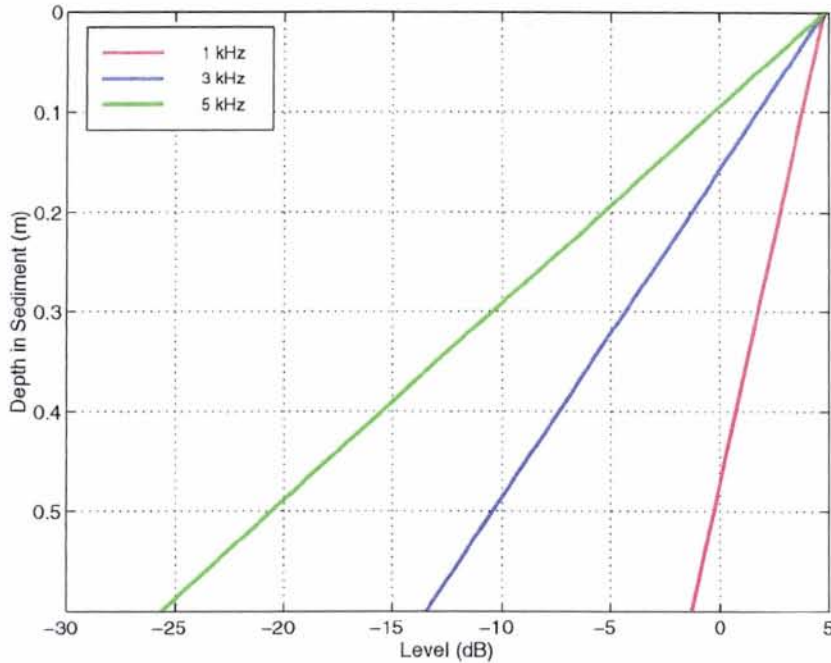


Figure 2 Example of SPL in a typical sandy sediment due to unit amplitude harmonic plane wave insonification at subcritical grazing ($c_w = 1530$ m/s, $c_s = 1685$ m/s, $\rho_s = 1.92$ g/cm³, $\alpha_s = 0.5$ dB/ λ , and $\theta_g = 18^\circ$).

wave in the bottom propagating parallel to the interface and decaying exponentially with frequency and depth into the sediment (see [3] for details).

Assumed here is a simple example of a harmonic plane wave with unit amplitude pressure insonifying a plane fluid-fluid interface (simulating a water-sediment boundary) with parameters: $c_w = 1530$ m/s, $c_s = 1685$ m/s, sediment density $\rho_s = 1.92$ g/cm³, sediment attenuation $\alpha_s = 0.5$ dB/ λ , and grazing angle $\theta_g = 18^\circ$. Figure 2 shows the SPL in dB as a function of depth into the sediment for frequencies 1, 3, and 5 kHz. Note that the transmission coefficient is greater than one for grazing angles near the nominal critical angle ($\theta_c \approx 24.8^\circ$ here), hence the levels are greater than 0 dB for some shallow depths in the sediment. It can be seen from the trends in this plot how higher frequency sonars (on the order of tens of kHz) will be very limited as to how much energy they can deliver to a completely buried target at subcritical grazing.

It should be noted that recent theoretical and experimental studies have shown that for subcritical grazing angles, scattering due to superimposed surface roughness on an otherwise flat water-sediment interface may, to a main extent, explain SPL's in the sediment in excess of what one would expect for the evanescent contribution on the flat surface alone. Maguer *et al.* [7] and Pouliquen *et al.* [8] show distinct frequency

regimes in the transfer function associated with subcritical transmission across the interface, such that the scattering mechanism dominates above 5–7 kHz and the evanescent contribution dominates at lower frequencies (for the specific bottom type examined in those works). Whether this higher frequency scattered (and hence incoherent) sound field that reaches the target at subcritical insonification can be taken advantage of for detection purposes (in mono- and/or multistatic geometries) is a topic for future study.

2.2 Scattering from buried targets

There has been a significant amount of research in recent years regarding the scattering characteristics of buried objects. Much of it has investigated the nature of scattering from buried elastic bodies, which can exhibit *resonance* features that may be useful for classifying buried objects. Lim *et al.* [9] have shown theoretical and experimental results for evacuated spherical shells. Using the T-matrix approach they examine theoretically the effect of burial on the amplitude and location in frequency of various resonant characteristics of elastic shells. Their experimental data, taken at near-normal incidence ($\theta_g = 74.6^\circ$), compares well with the theory. Tamašauskas and Fawcett [10] have extended this work with a simulation sensitivity study, examining the effects of varying sediment parameters, grazing angles, burial depth, and of rescattering terms. When compared to free-field (in water) scattering models, the results of this work show frequency shifts in certain resonance phenomena due to the higher sound speed in the sediment, and damping of higher frequency components due to the higher attenuation coefficients of the sediment.

While the above cited works consider buried spheres due to the tractability of the solutions, cylindrical objects are also of interest, especially for mine countermeasures applications. Some of the most recent work on scattering by buried cylinders has been done by J. A. Fawcett at SACLANTCEN [11, 12], where infinite cylinders at broadside aspect have been considered. Although not dealt with explicitly in a detection context, especially relevant for the work here is the simulation [12] of completely buried elastic cylinders insonified at subcritical grazing angles. A drastic falloff in echo level is shown for higher frequencies (regardless of the effects on the resonances) due to the depth and frequency dependence of the incident evanescent wave traveling in the sediment. Also, the effects of rough interface scattered sound in the sediment on target scattering characteristics is preliminarily dealt with in [11].

In addition to their work with resonance effects, Lim *et al.* [9] also comment on the possibilities for long-range detection of buried shells, and the role of evanescent insonification. They simulate both elastic spherical shells and rigid spheres at various burial depths, grazing angles, and for cases of $ka = 8$ and 2. The results of these simulations show that there should be possibilities for receiving large amplitude

target returns at subcritical grazing, and that the lower frequencies provide a better chance of this given the higher amplitude of the evanescent field in the sediment.

Rogers [13] has theoretically investigated the use of frequencies in the Rayleigh scattering region ($ka \approx 0.2$ to 0.5) in order to detect buried targets. One significant finding of this work is an increase in *effective* target strength for targets buried in common ocean sediments for moderately subcritical grazing angles. Effective target strength is referred to here because changes in the incident pressure field associated with transmission across the water-sediment boundary are included in the target strength of the buried object for comparison to the target strength of the same object in water. By modeling various cases of target and sediment parameters, along with reverberation modeling (to be discussed in Subsect. 2.3), it was found that relatively high SNR's can be achieved in this frequency range.

Recent work by Schmidt [14] describes the incorporation of target scattering capabilities into the OASES-3D scattering and reverberation model [15, 16]. The target is treated as a virtual source with a radiation pattern calculated by convolving the incident field with a target scattering function. The target scattering function can be calculated analytically for some canonical shapes (such as spheres), or it can be calculated numerically for general targets. Figure 3 shows the resulting relative echo levels vs. frequency for a rigid "flush" buried sphere (i.e., buried just to the point where it is completely covered by sand) of radius $a = 0.3$ m using OASES-3D (the sediment parameters are the same as those used for generating Fig. 2). In agreement with the previously cited work, it can be seen that echo levels decrease dramatically with increasing frequency for subcritical insonification. In the supercritical case, the oscillations in level are due to the usual interference from the creeping wave seen in the frequency regime $1 < ka < 10$ [17]. The smaller scale fluctuations at higher frequencies for the subcritical case are numerical effects in the model computation.

It should be noted that since the evanescent wave is inhomogeneous (i.e., its amplitude is not constant along its constant phase front), and target strength relationships for $ka \ll 1$ and $ka \gg 1$ must be used with care in this transitional ka range, simple approximations to the echo level vs. frequency are not immediately obvious. It should be possible, however, to arrive at parameterized versions of these curves for simple shapes given the current level of simulation capability.

2.3 Bottom backscatter

Bottom backscattering strength (BBS) is dependent on the geomorphological and geoacoustical properties of the seabed, the grazing angle, and the acoustic frequency. The physical mechanisms responsible for bottom backscattering are rough surface scattering at the water-sediment interface and scattering due to inhomogeneities within the volume of the sediment.

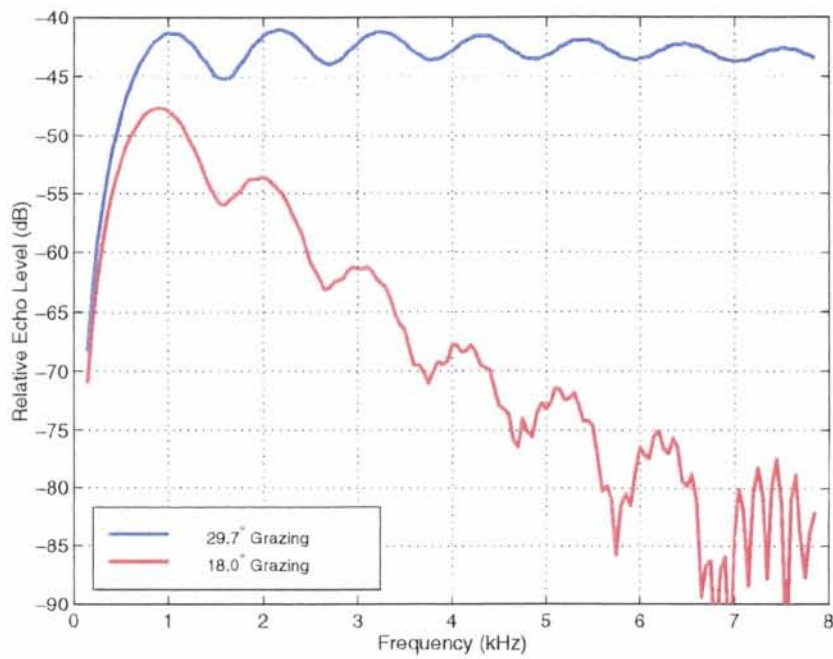


Figure 3 Relative echo levels for a flush buried sphere ($a = 0.3$ m), insonified above (blue) and below (red) critical angle ($c_w = 1530$ m/s, $c_s = 1685$ m/s, $\rho_s = 1.92$ g/cm³, and $\alpha_s = 0.5$ dB/ λ).

Over time, a number of efforts have been made to model and experimentally measure this important sonar parameter for use in sonar performance prediction. Historically, relatively simple relationships for BBS vs. grazing angle have been used, such as the well-known Lambert's rule, $BBS = 10 \log(\mu \sin^2 \theta_g)$, where μ is typically adjusted depending on a loosely defined bottom type (i.e., sand, mud, gravel, etc.). Lambert's rule is based on rough surface scattering theory [17], and rarely provides a good fit to observed data taken over a wide range of grazing angles and/or frequencies, especially when sediment volume scattering plays a significant roll in the overall BBS. Various theoretically- and empirically-based methods have been suggested for modifying Lambert's rule in order to more accurately model BBS [18, 19, 20].

In recent years, more complex models that incorporate more physics-derived computational approaches (and hence require more information about the structure and properties of the seabed) have been proposed. Among these are the high frequency (10–100 kHz) model of Mourad and Jackson [21], their extension of the model to include volume scattering at lower frequencies (100–1000 Hz) [22], and the work of Lyons *et al.* [23] which handles sediment volume scattering by accounting for scattering from subbottom interfaces and an inhomogeneous continuum.

Another recent step forward in modeling acoustic interaction with the seabed has been to develop modeling schemes that use realizations of seabeds with given statistics in order to calculate the backscattering characteristics in the time or frequency domains. In this way the complex interactions are not reduced to a single number (BBS), and time and frequency domain statistics of the reverberation can be examined. Examples of this type of approach are given by Pouliquen *et al.* [24] and Schmidt *et al.* [16].

Given the high degree of frequency dependence seen in the target scattering from the last subsection, it is worthwhile to try to identify trends in frequency dependence for BBS at low grazing angles, especially for subcritical insonification. Ideally, a flexible model that has been experimentally validated over (roughly) the decade of frequency from 1–10 kHz would provide what is needed. To the authors' knowledge, this type of modeling capability does not exist. Therefore, published data sets and modeling efforts must be relied on. Here, subcritical grazing angles will be emphasized.

One generalization that can be made is that as frequency increases, sediment volume scattering will play less of a role to total BBS due to the rapid attenuation of the higher frequency transmitted sound at subcritical grazing angles. Its contribution at lower frequencies will be highly dependent on the structure of the seabed, for the most part on the depth and composition of underlying substrata (although the roles of velocity and density gradients can not be completely dismissed). Since objects that are completely buried in sand-type sediments are of primary concern, however, we must assume that there is a sand layer at least one object diameter thick (~ 0.5 m) before any significant substrata. For grazing angles well beyond

critical, this will limit significant levels of sound transmitted to this depth to the very lowest frequencies.

For scattering from the rough water-sediment interface, there is evidence for a decrease in level with decreasing frequency. In the composite roughness model used by Mourad and Jackson, this is because the surface “appears” rougher on finer scales. In practice, though, this will depend on the overall roughness spectrum of the bottom being considered.

Therefore, what general conclusions can be made about total BBS for subcritical grazing angles in the frequency range 1–10 kHz? Unfortunately, a situation exists where the two mechanisms contributing to the overall backscattering level have opposite frequency dependencies. A best-case scenario can be imagined, however, where the sand layer is deep and homogeneous, providing no significant sediment volume scattering, and with a roughness spectrum characteristic of the composite roughness model. There would, therefore, be seen an increase in BBS with frequency, giving low “noise” levels (bottom backscatter) where the “signal” level (target echo) is high. Worst-case scenarios would probably give a relatively frequency independent BBS. This uncertainty underscores the need for accurate methods of determining seabed structure and geoacoustical parameters, and for validated models for predicting seabed scattering characteristics in order to accurately predict sonar performance for a wide range of environments.

3

Experiment description

A field trial was performed during November-December 1997 (designated MCG2-97) in order to study acoustic penetration into a sandy seabed and acoustic backscattering characteristics of proud and buried targets at low grazing angles, all in the approximate frequency range 2-16 kHz. This report focuses on the buried target data. The remainder of this section will detail the equipment used during the trial, the location and environmental conditions, the targets used, and the trial geometry.

3.1 Location and environment

The site for the trial was Marciana Marina, off the north-central coast of Elba Island, Italy (approximate Lat.-Lon.: 42°48'35" N, 10°12'00" E). This site provided a relatively sheltered area with a gently sloping bottom. The water depth was between 12.0 m and 14.5 m in the working area of the experiment. Sub-bottom profiling showed roughly 9 m of sand over bedrock. Core measurements over the top 30 cm of sand showed somewhat mixed grain size results, with mean grain sizes (measured over 5 cm segments) varying in the range $\phi \approx 0.7$ to 1.8 ($\phi = -\log_2 d$, where d is the grain size diameter in mm). Sound speed in the sediment was measured at roughly 1710 m/s (from laboratory measurements at 200 kHz, with measurement error estimated at ± 3 %). Sound speed profiles taken in the water column during the experiment showed isovelocity conditions at 1515 m/s.

Figure 4 is a picture of the ripple structure on the bottom taken from an underwater digital video camera. The cables seen in the picture lead to buried hydrophones used for another portion of the trial (the overall layout of the equipment will be covered in Subsect. 3.4). Diver measurements and stereo photogrammetry results taken on the area give similar estimates of the ripple height at $\sim \pm 3$ cm (peak to trough), and a dominant ripple periodicity of wavelength ~ 25 cm.

3.2 Equipment

The acoustic source used for this experiment was the TOPAS PS 040 [25] parametric sonar [26]. With a primary carrier of 40 kHz, this parametric source provides ade-



Figure 4 *Picture of bottom ripple structure with buried hydrophone array.*

quate secondary generation in the frequency range 2–16 kHz. The secondary source levels (calculated by integrating over the total secondary bandwidth) are over 200 dB re 1 μPa @ 1m (see [27] for details). The use of the parametric source allows relatively narrow transmit beams (on the order of 3.5° , also integrated over the band) for the secondary frequencies.

One type of secondary waveform generated by the TOPAS is the so-called “Ricker” pulse, which is defined as the second derivative of a Gaussian function [28]. An example in the time and frequency domains is given in Fig. 5. These pulses have a time-bandwidth product close to one. The data runs analyzed in this report will consider only this transmit pulse type.

The receiver was a 16-element linear array whose preamplifier section was specially designed to reject the primary frequency band of the TOPAS (note that the primary frequency source levels for this parametric source are roughly 30 dB greater than for the secondaries). The elements were spaced at 9.4 cm, giving a nominal $\lambda/2$ spacing for 8 kHz. The array was mounted vertically close to the source giving a near-monostatic source-receiver geometry, and allowing moderate rejection of scattered energy coming from the sea surface.

In order to easily vary aspect and grazing angles, a portable underwater rail system was designed and built [29] for the above-mentioned transmit-receive system. It consisted of a 24 m long rail that rested on the seabed, and a four-footed basement structure on which an adjustable-height tower was attached. The TOPAS and the 16-element array were mounted in a frame with mechanical pan and tilt motors at the top of the tower. While the TOPAS source could be mechanically steered in both pan and tilt, the vertical array was attached to the frame such that it could not be tilted in the vertical, only panned in the horizontal. The entire basement-tower

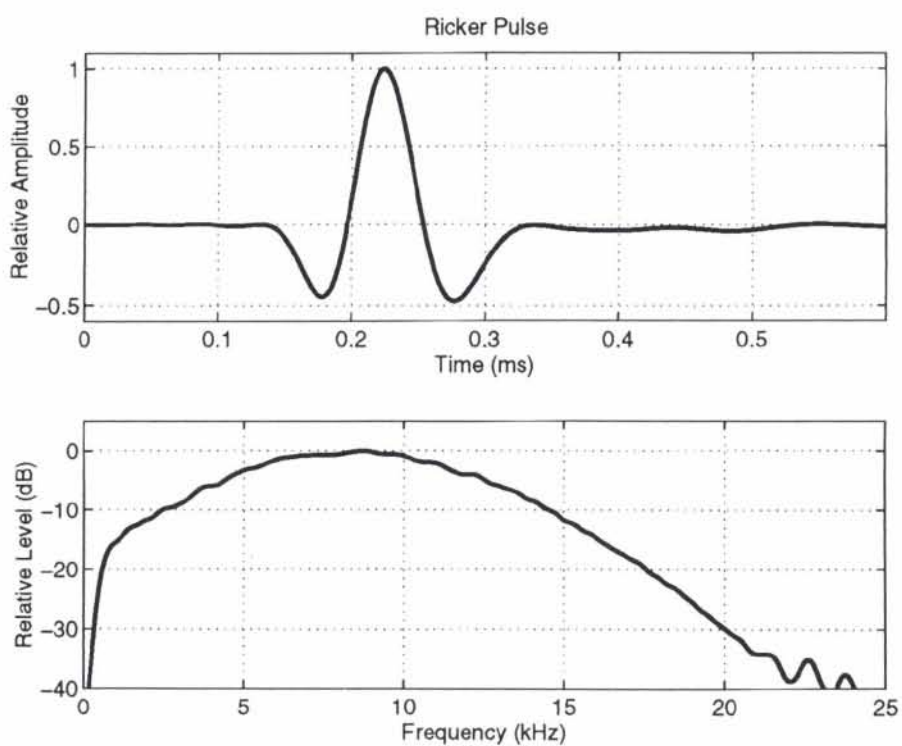
SACLANTCEN SR-293

Figure 5 Example of a TOPAS-generated Ricker transmit pulse in the time (top) and frequency (bottom) domains.

SACLANTCEN SR-293

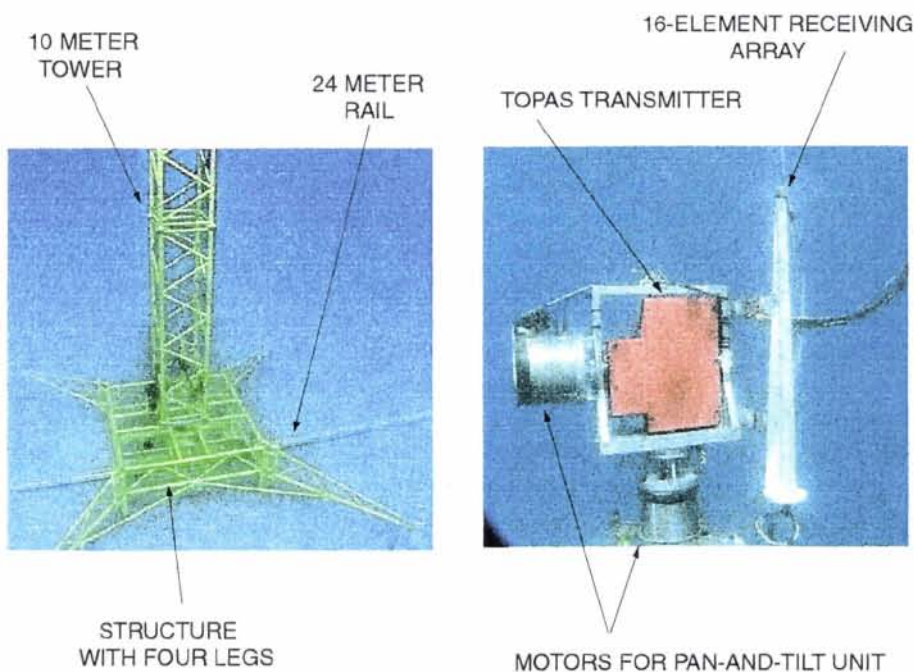


Figure 6 *Equipment used for trial: rail, stabilizing structure, and tower (left); transmitter, receiver, pan-and-tilt system (right).*

assembly could be lifted off the seabed by pumping air into reservoirs attached to the tower, and could be moved along the rail by the use of an electric motor and a chain assembly. Underwater photographs of the equipment can be seen in Fig. 6.

All underwater equipment was deployed ~ 150 m offshore and cabled to a shore station. The received signals were appropriately filtered, amplified, and recorded on a workstation-based data acquisition system. The data were written directly to binary files on hard disk, and immediate data quality checks could be done using computers linked together over a small local network.

3.3 Targets

The two buried targets used during the trial were a solid aluminum sphere and a water-filled cylindrical shell. The solid aluminum sphere had a radius of 0.3 m, and has been used as a reference object in other theoretical/experimental work at SACLANTCEN [30]. The cylindrical shell was made of steel 6 mm thick, was 2.0 m long, had radius 0.25 m, and had flat endcaps. This cylinder has also been used as a reference object for various theoretical and experimental studies [31, 30].

Both targets were intended to be flush buried (as described in Sect. 2.2). This is an important case, since in addition to the targets being optically invisible, it is also generally considered the limiting case for scour burial mechanisms on sandy seabeds. Scour pits are formed around bottom-laid objects due to sediment transport which is dependent on the characteristics of the seabed and the hydrodynamic flow velocity [1]. Bottom-laid objects provide a flow obstruction which can locally enhance the flow velocity, and create conditions for sediment transport. Once an object has settled into a scour pit and the pit has been filled by sedimentation such that the object is completely covered, the flow is no longer perturbed and scouring can be assumed to cease.

In order to bury the targets for this trial, pits were excavated by divers, the targets placed in the pits and then re-covered with sand. The resulting burial had the tops of the targets between 10 and 15 cm from the sand-water interface. Unfortunately, time was not available in order to allow the seabed to return to a more natural state. Future experiments have been planned with this objective in mind.

Reference hydrophones were attached to the buried targets in order to have a precise estimate of the direct travel time of the transmitted pulses. These hydrophones were important both for overall geometry reconstruction (especially grazing angle calculation) and for estimating the expected time of arrival for the target returns.

3.4 Geometry and equipment layout

Figure 7 shows a top view of the experimental layout for the trial. The geometry was designed in order to obtain target backscattering measurements for transmit-receive geometries both above and below the nominal critical angle of the sediment. An array of hydrophones was also buried during this experiment in order to measure the one-way transmission levels of sound into the sediment; these data will be discussed in another report. The water-filled cylinder was buried such that its orientation with respect to the rail was as close as possible to broadside in order to maximize its effective target strength.

There was a noticeable slope ($\sim 4.6^\circ$) to the bottom along the line of the experimental setup. An approximate schematic for the side view is shown in Fig. 8. The source and receiver were mounted on a 10 m tower, also shown in Fig. 8.

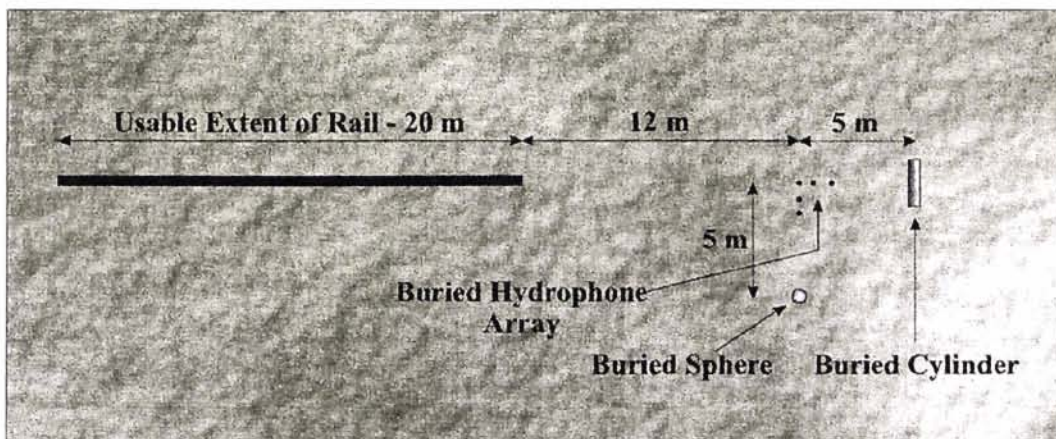


Figure 7 Top view of the experimental geometry for MCG2-97.

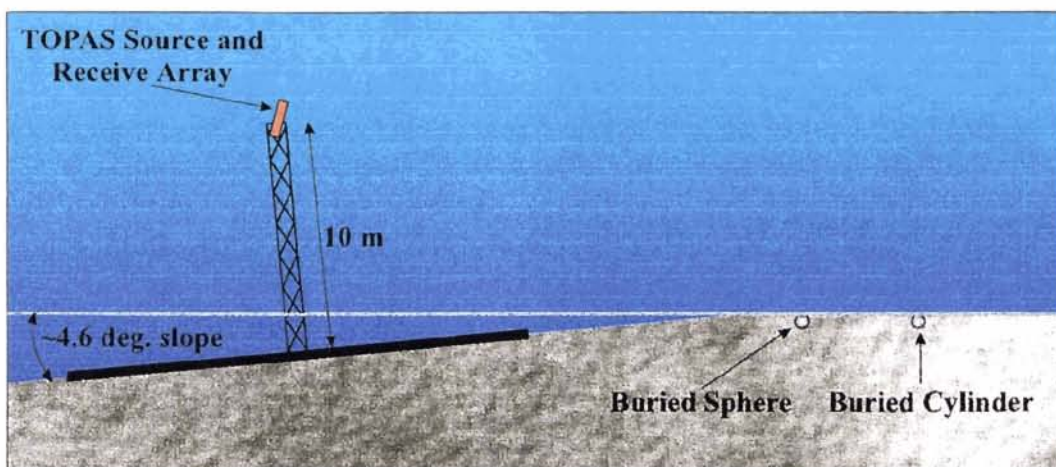


Figure 8 Side view of the experimental geometry for MCG2-97.

4

Data analysis

4.1 Basic data description

In order to study the buried target backscattering characteristics as a function of grazing angle, the tower was moved along the rail to a given position, the source was steered to a particular target based on an estimate of the experimental geometry (and using the signal on the hydrophone attached to the target as an additional guide), and a series of pings were transmitted and the backscatter recorded. As mentioned previously, the transmit pulse was the Ricker pulse shown in Fig. 5. The pulse repetition rate was typically set to 500 ms. Figure 9 shows an example of time series recorded on the 16-element array for the buried sphere with a grazing angle of 33.3° .

In Fig. 9, the bottom-most hydrophone on the array is labeled number 1 and the top-most element is number 16. The direct sphere return can clearly be seen arriving between ~ 21 – 22 ms across the array. The other return arriving between ~ 25 – 26 ms is due to energy that has scattered from the sphere up to the water surface and back down to the receive array. Note that the return from the surface is less coherent across the array due to the rough nature of the sea surface. Channel number 17 on the plot is from the hydrophone that was attached to the buried sphere.

An important tool used for experimental data quality checks, post-processing, and analysis is a conventional plane wave delay-and-sum beamformer (see [32] for details). Figure 10 shows a beamformed image for the ping of Fig. 9. In this plot, a steering direction of 90° corresponds to broadside to the array, angles greater than 90° point toward the sea bottom, and angles less than 90° point toward the sea surface. The direct target echo and surface reflection can be seen at the times corresponding to those seen in Fig. 9.

4.2 Ping-to-ping fluctuations

Although the tower and rail provided a relatively stable platform for easily varying the grazing angle to the buried targets, the tower was not perfectly stationary in the vertical while at a given rail position due to wave action. Figure 11 shows

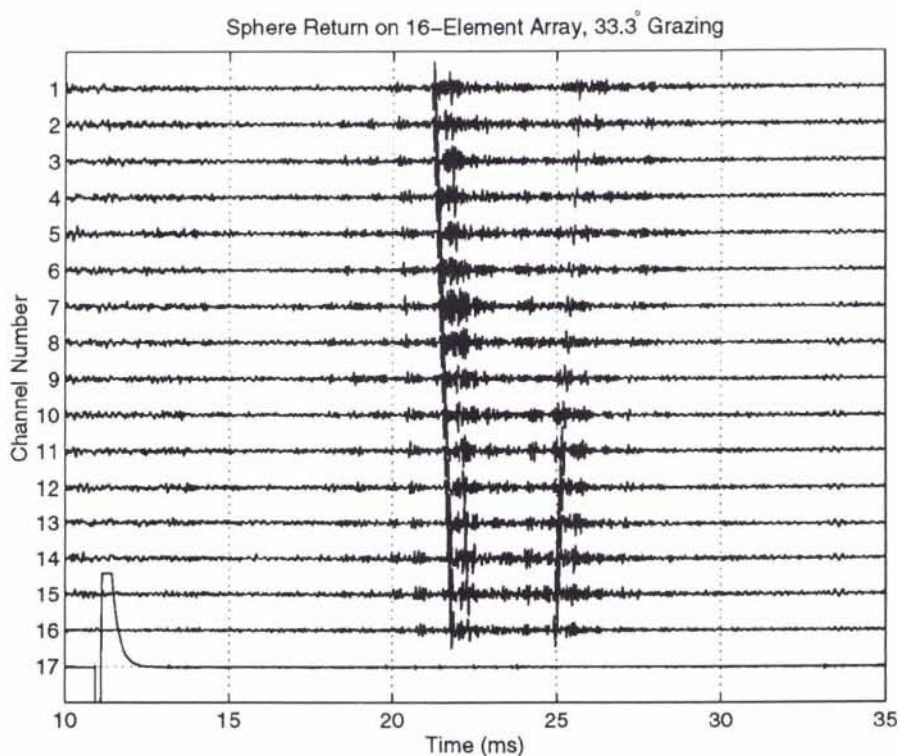


Figure 9 Example of 16-channel array reception for buried sphere at 33.3° grazing. The bottom-most channel of the array is labeled #1, the top-most #16. Channel #17 is from the hydrophone attached to the sphere.

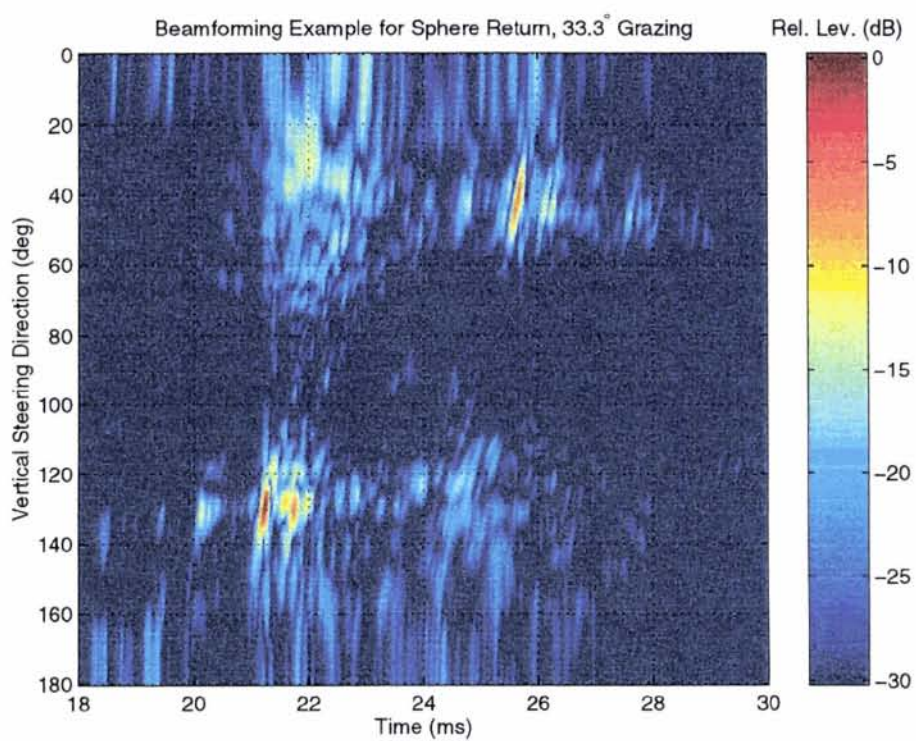
SACLANTCEN SR-293

Figure 10 Example of beamforming output for buried sphere ping at 33.3° grazing. Broadside corresponds to 90° vertical steering.

SACLANTCEN SR-293

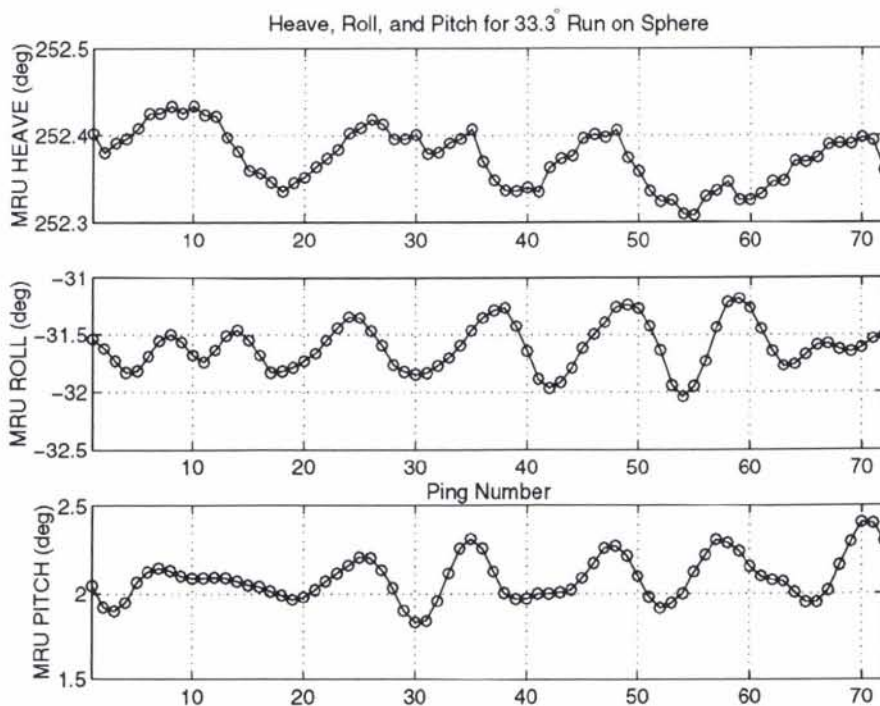


Figure 11 Example of Motion Reference Unit (MRU) data for buried sphere run at 33.3° grazing.

an example of the variability in sonar position during a given run (this is the run from which the single ping in Fig. 9 was taken). A Motion Reference Unit (MRU) was attached to the sonar head so that its overall attitude could be measured on a ping-by-ping basis. The “heave” measurement corresponds to heading in degrees relative to magnetic north. If one considers looking straight through the sonar head from behind, the “roll” measurement corresponds to backward-forward tilting in degrees of the sonar (negative “roll” corresponds to a forward tilt), and the “pitch” measurement corresponds to clockwise-counterclockwise rotation in degrees of the the sonar. The result of the wave action contributing to the tower movement can be clearly seen in the roll and pitch traces of Fig. 11. The variability seen here is representative of the runs to be shown in this report.

Another source of ping-to-ping fluctuation in this data set is due to backscatter coming from the surface. Since the surface was changing in time due to wave motion, it provided a different surface for the energy coming from the target to scatter from on each ping. Although the beamformer is able to reject energy arriving from unwanted directions to a certain extent, it can not do this perfectly. This is illustrated in Fig. 12, which shows the extracted direct target returns for six different pings. These time series correspond to the beam that contains the maximum target return, chosen from a small subset of beams near the estimated grazing angle. Note that

SACLANTCEN SR-293

the direct target return from 21–22 ms is very consistent across pings, but that the shape of the return from 24–25 ms is variable. This is “sidelobe” energy from the surface return.

It should be noted that this energy coming from the surface reflection may, in addition to the direct return, be important for buried target detection. Fawcett [11] and Hovem [33] have recently shown simulation results indicating that more energy can be backscattered from buried targets in directions closer to the vertical than in the monostatic direction. Whether this energy is received after reflection from the sea surface in a monostatic configuration or directly in a multistatic mode, and the relation of the multistatic target echo level to reverberation level (also dealt with in [33]) are items for future work.

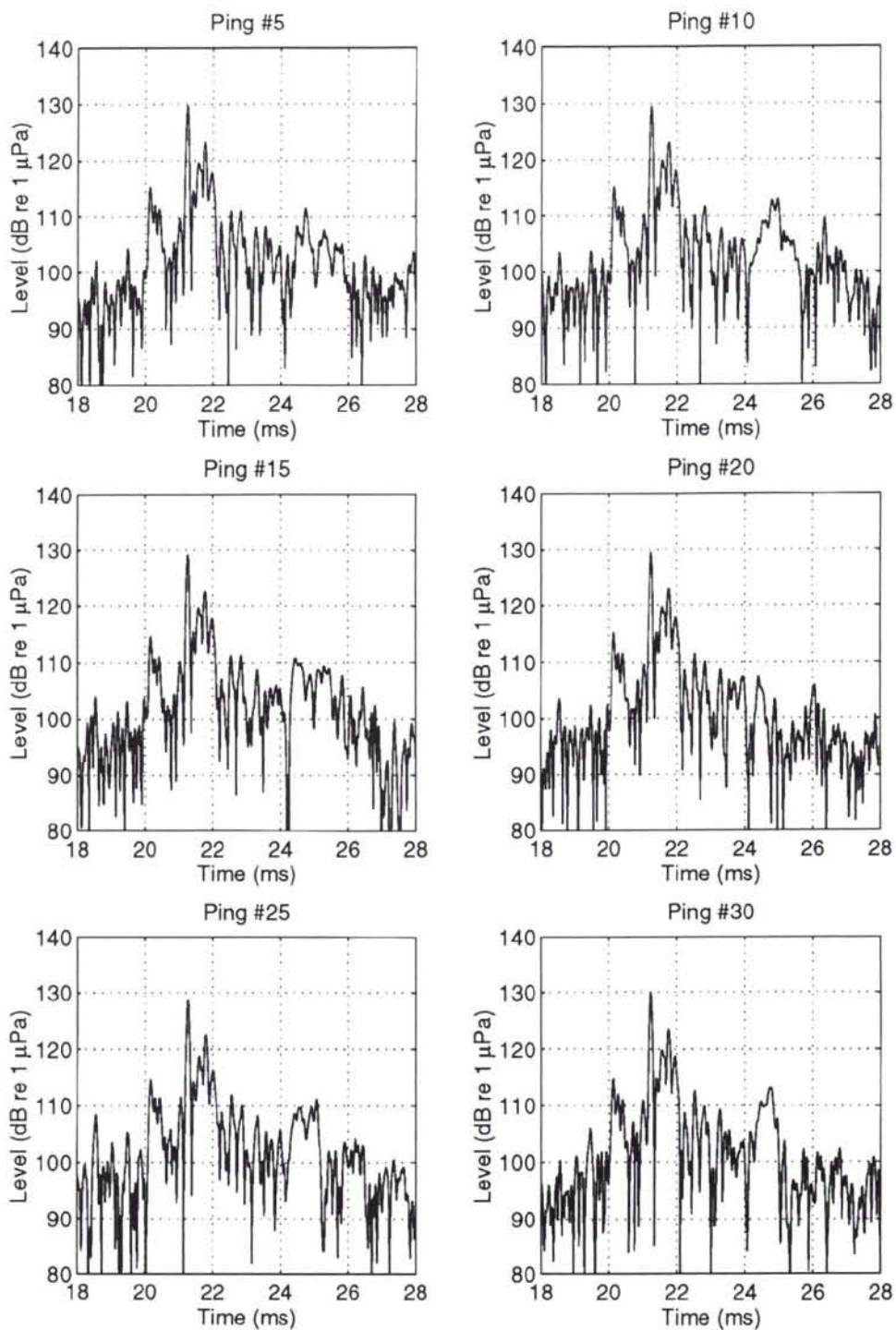


Figure 12 *Extracted target returns for various pings of the buried sphere run at 33.3° grazing.*

4.3 Full band results

Figures 13 and 14 show plots of extracted target returns for the buried sphere at the various grazing angles covered in the experiment. Again, these represent the beam outputs that contain the maximum target return. The small arrows at the tops of the plots show the estimated time of arrival for the target echo based on the direct path travel time measured by the hydrophone on the target.

The background estimates were formed using the order truncate average (OTA) method [34] with a 5 ms averaging window (giving roughly 39 independent samples). Background normalization and design of constant false alarm rate (CFAR) processors in cases such as this is a difficult problem [35] given the nonstationarity of the reverberation and the likely departure from Gaussian of the reverberation statistics (as described in [36]). The OTA method mentioned was chosen for this analysis as a trade-off between complexity and performance, and is meant only to allow consistent comparisons of SNR estimates for the various targets, grazing angles, and frequency bands. Optimization of this important processing step is an item of future work.

Figure 13 shows relatively good estimated SNR down to $\theta_g = 25.5^\circ$. Unfortunately, the sand floor in the experimental area was not completely clean, and the echo from a small partially buried rock is visible in the returns shortly before (~ 1 ms) the sphere. Figure 14 shows decreasing SNR, until the sphere echo is indistinguishable from nearby reverberation peaks at $\theta_g = 21.9^\circ$.

Figures 15 and 16 show in a similar light the results for the buried cylinder. In this case, there is also some “extra” clutter arriving before the target echo, mainly due to the buried hydrophone array and its cables. The echo from the cylinder is relatively clear at the first few grazing angles, but becomes obscured fairly quickly (by $\theta_g = 22.2^\circ$). Interestingly, the target echo appears to reemerge slightly from the surrounding noise at the two lowest grazing angles, which could be due to a more rapid falloff in BBS than target echo level vs. grazing angle. Also, there is a consistent feature in the returns of Fig. 16 appearing ~ 4 ms after the target echo. This has been identified as a reflection from an unknown bottom object (possibly buried) through examination of the full beamformed images, rather than surface reflected energy.

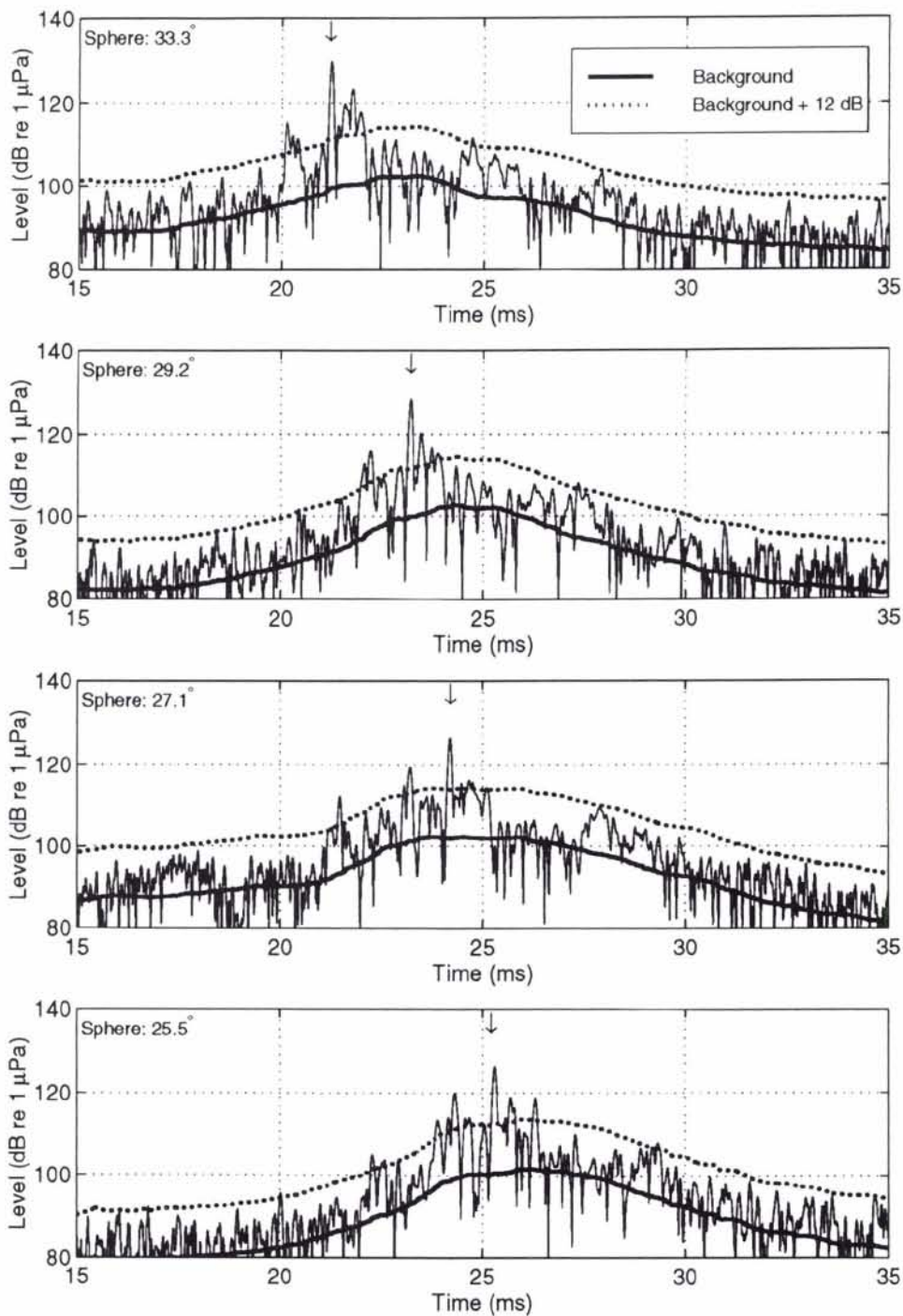


Figure 13 Sphere returns (full band) for four highest grazing angles with background estimate.

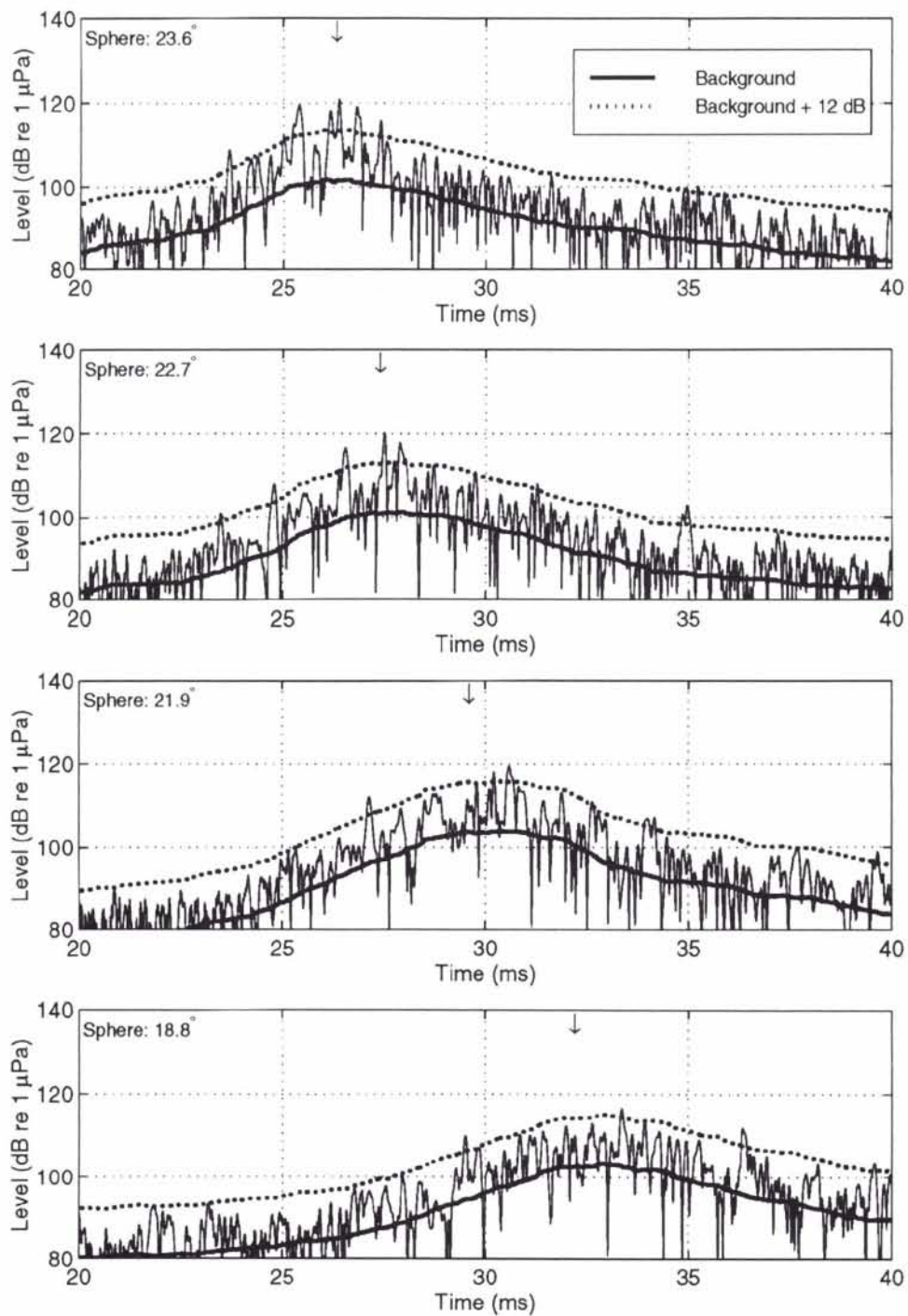


Figure 14 Sphere returns (full band) for four lowest grazing angles with background estimate.

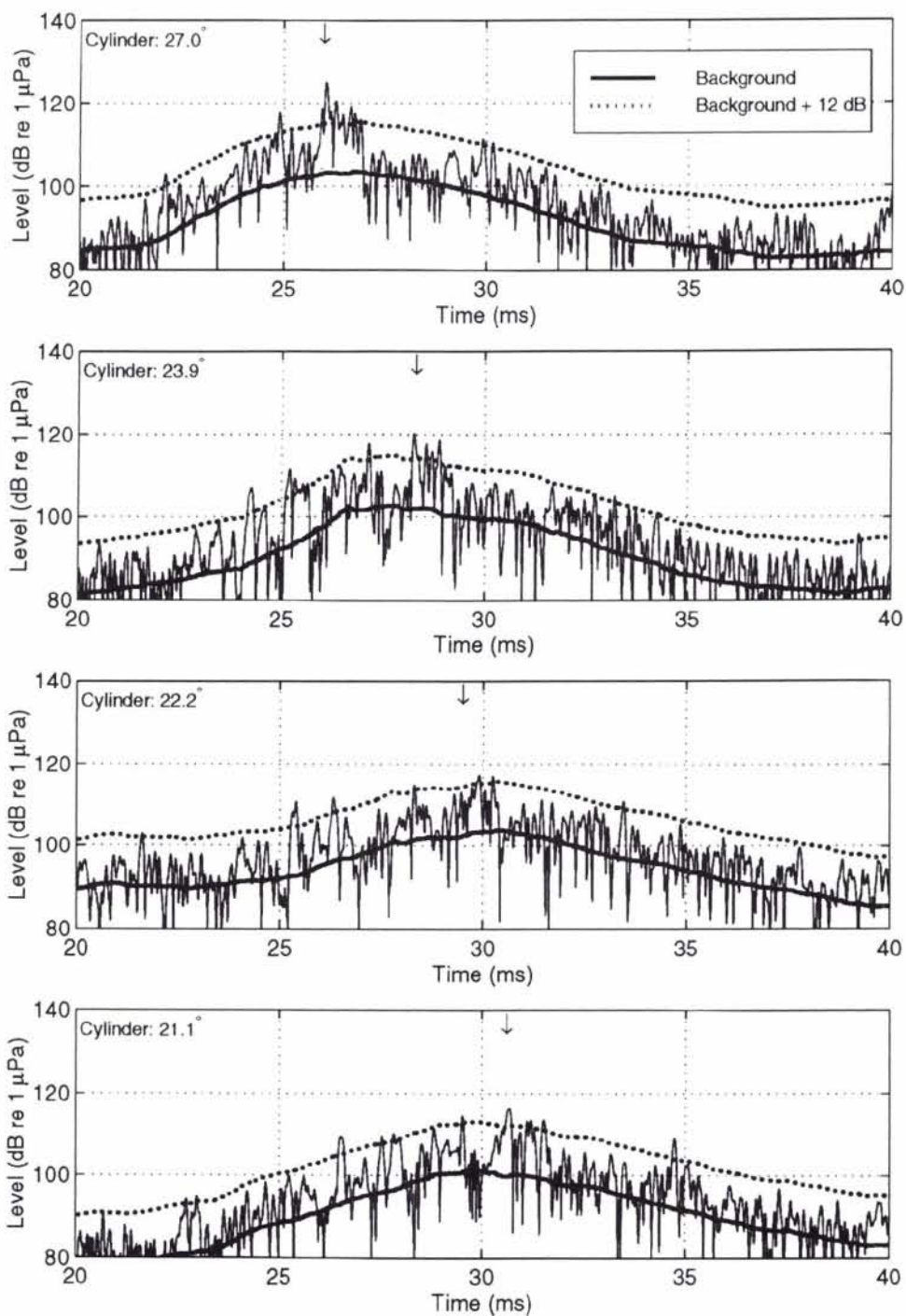


Figure 15 Cylinder returns (full band) for four highest grazing angles with background estimate.

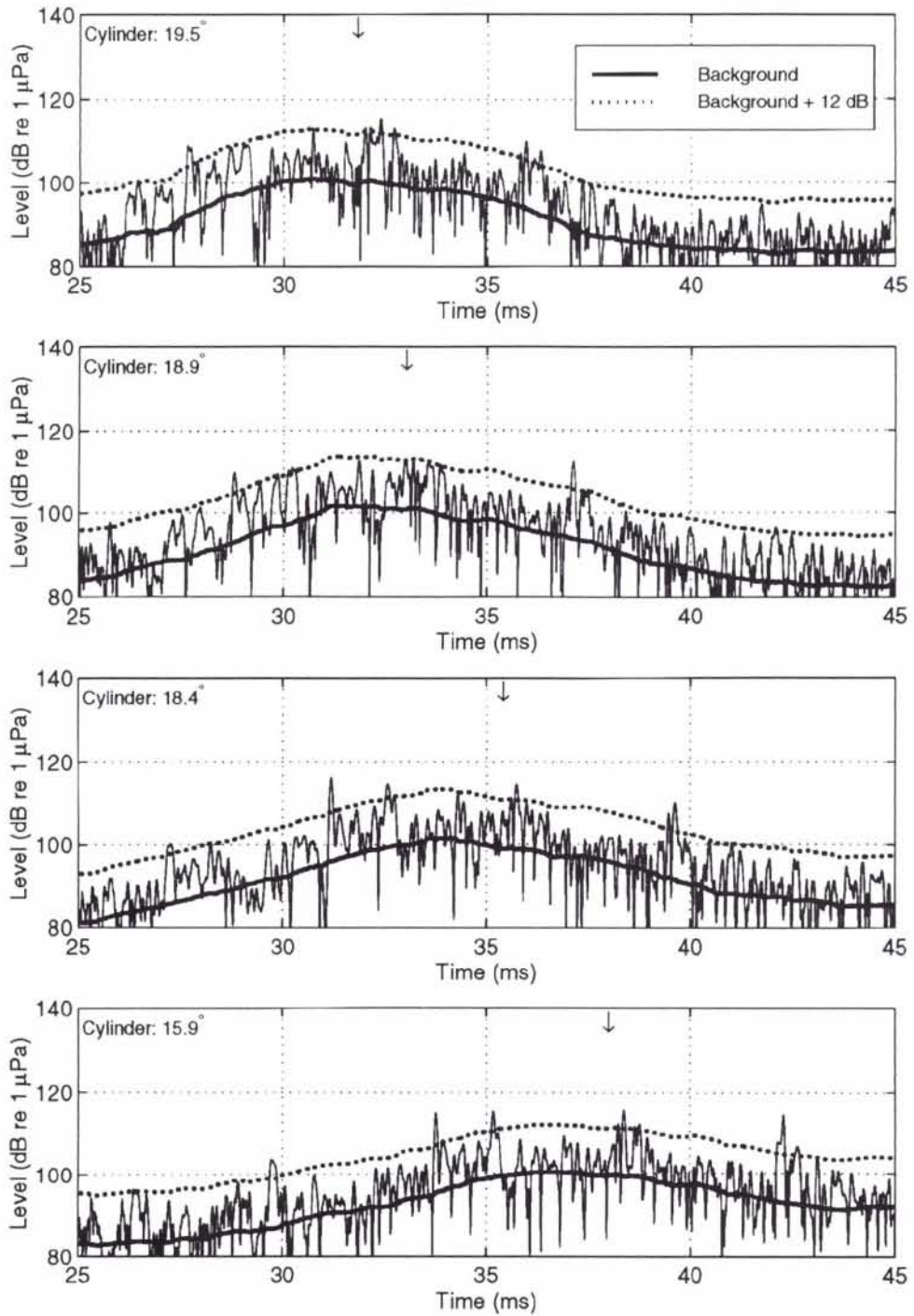


Figure 16 *Cylinder returns (full band) for four lowest grazing angles with background estimate.*

4.4 Low frequency processing and noise limitation

In order to get an initial indication of the frequency dependence of the combined target echo plus “noise” signal, the data have been processed by applying a lowpass filter at 3 kHz. This is done simply to show that an improvement in SNR can be obtained at subcritical grazing angles by concentrating on the lower frequencies, as would be expected from the results of Sect. 2. Optimization of transmit pulses, transmit and receive beamwidths, and receiving filters will be follow-on topics of research.

As can be seen from Fig. 5, the low frequency levels of the given transmit pulse are falling off quite rapidly below 3 kHz. When applying the lowpass filter to the data, it was found that the target echoes are more likely “noise” limited (ocean ambient and electronic) instead of reverberation limited. This is illustrated in Fig. 17 with the run on the sphere at $\theta_g = 25.5^\circ$.

The top plot in Fig. 17 shows the full band results, where the ambient levels can be seen to be well below the backscattered levels in the important region around the target echo. The ambient data is taken from a beam steering in the same direction as the backscatter data. Since the ambient data were found to be rather nonstationary due to transients in the water from equipment movement, levels averaged *incoherently* (i.e., averaging the envelope squared) over 50 ping intervals are shown vs. the single ping backscatter results. The middle plot shows the lowpass filtered results. The averaged noise level is significant compared to the single ping target echo and the surrounding reverberation/noise peaks.

The desirable solution to this noise limitation would be to increase the source level to ensure a reverberation limited scenario. Since this is not possible with the given data set, *coherent averaging* has been used. The bottom plot of Fig.17 shows the result of coherently averaging the low frequency data over 50 pings (i.e., directly averaging the time series in volts).

Of some concern is the effect of the ping-to-ping fluctuation due to source/receiver movement on the coherent averaging process. From Fig. 11, maximum excursions of tower roll can be seen to be on the order of $\pm 0.5^\circ$. With a 10 m tower height, we can approximate the maximum lateral displacement at the source/receiver to be roughly ± 9 cm. The wavelength in water at 3 kHz is $\lambda_{min} = c_s/f_{max} \approx 50$ cm. Although the maximum excursions give approximately $0.36\lambda_{min}$ phase shifts which can lead to some destructive interference, this is not seen to be a large problem since most of the pings have smaller shifts. As an example, comparing the two bottom plots of Fig. 17 shows a loss of only a few dB between the single ping target echo level and that for the averaged case.

Unfortunately, the coherent averaging of the lowpass filtered data provides a differ-

SACLANTCEN SR-293

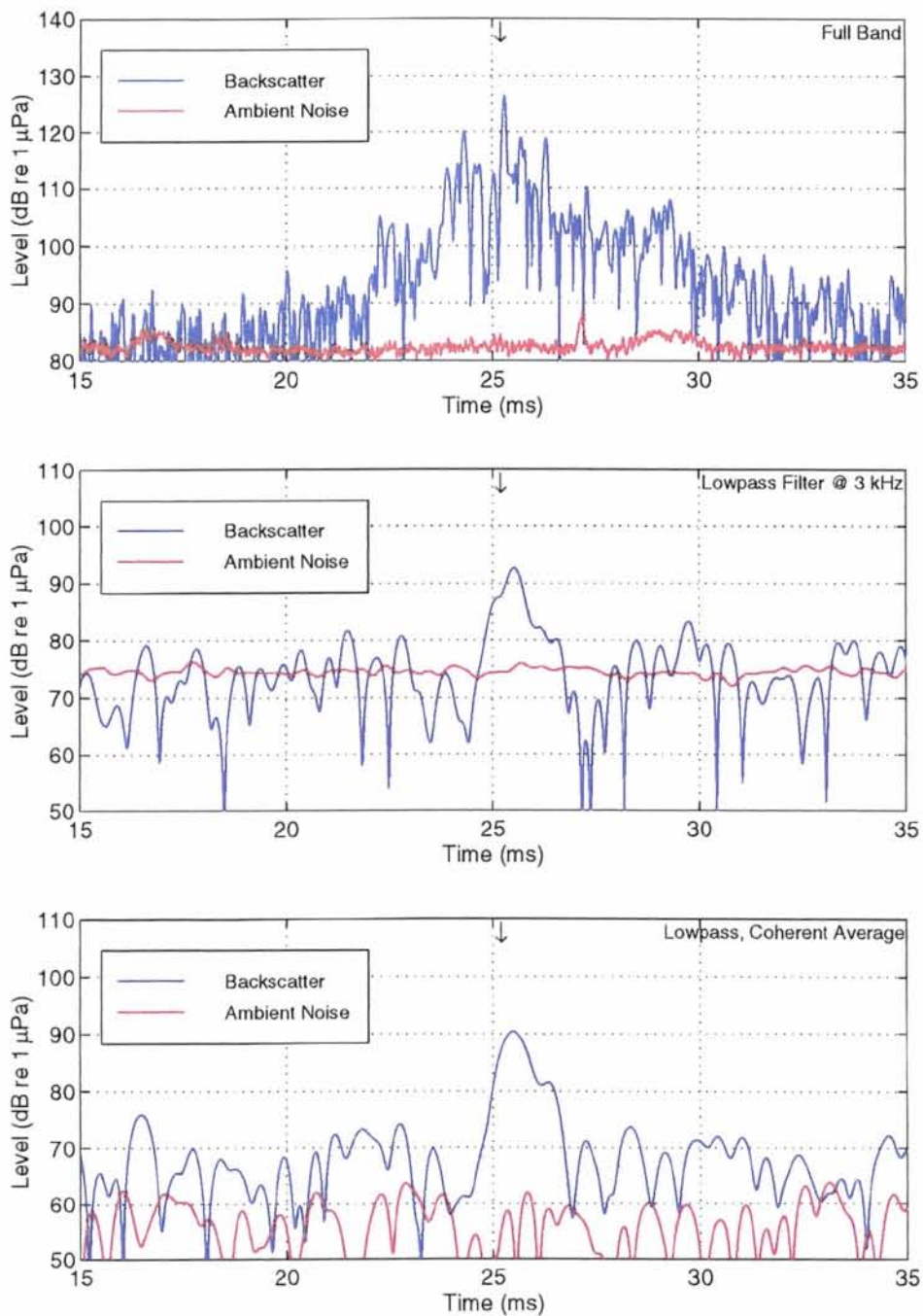


Figure 17 Backscatter data (sphere at 25.5° grazing angle) vs. characteristic ambient noise: single ping full band backscatter with incoherently averaged noise (top), single ping backscatter with incoherently averaged noise lowpass filtered at 3 kHz (middle), and filtered coherently averaged backscatter and noise (bottom).

SACLANTCEN SR-293

ent type of processing than the single ping target echoes of the last subsection where the full band data was considered. This should be kept in mind when comparing the results. However, given the previous fluctuation discussion and the spatial stationarity of the dominant bottom reverberators, the comparison should give a good initial indication of the frequency domain trends of the physical phenomena.

4.5 *Low frequency results*

Figures 18 and 19 show the results of lowpass filtering the returns at 3 kHz for the buried sphere, while those for the cylinder are shown in Figs. 20 and 21. The reduction in total bandwidth due to the filtering is apparent in the overall “smoother” appearance of the traces and the broadening of the target echo compared to the full-band results (where the target is evident). For lower grazing angles, a qualitative comparison between the full-band and filtered results shows that the target echoes are more evident amidst the noise background. For higher grazing angles, and especially for the highest grazing angles of the sphere, the full-band target echoes are more (or at least equally) apparent. Quantified SNR estimates and discussion of these results will be given in the next subsection.

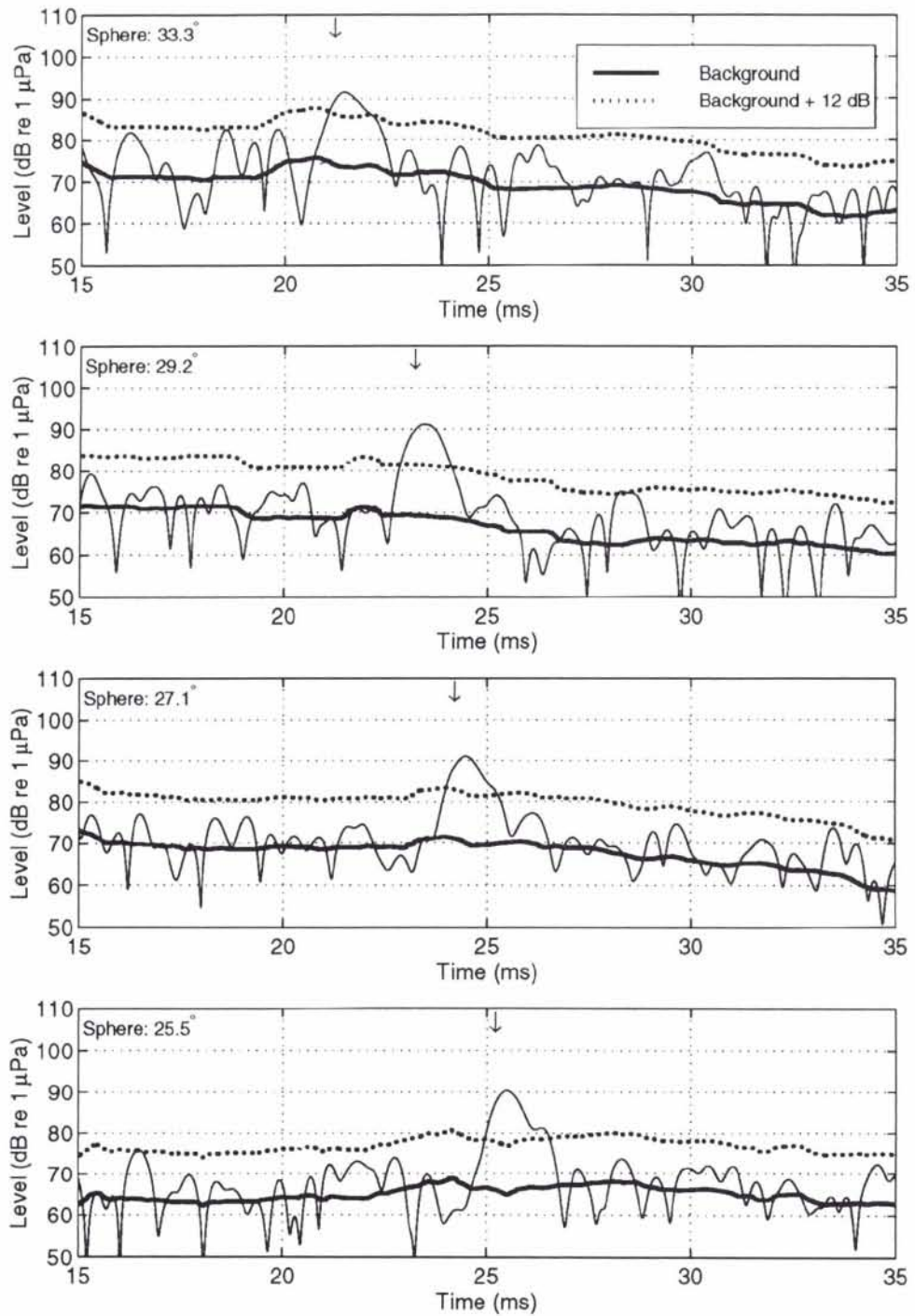


Figure 18 Sphere returns (lowpass filtered at 3 kHz) for four highest grazing angles with background estimate.

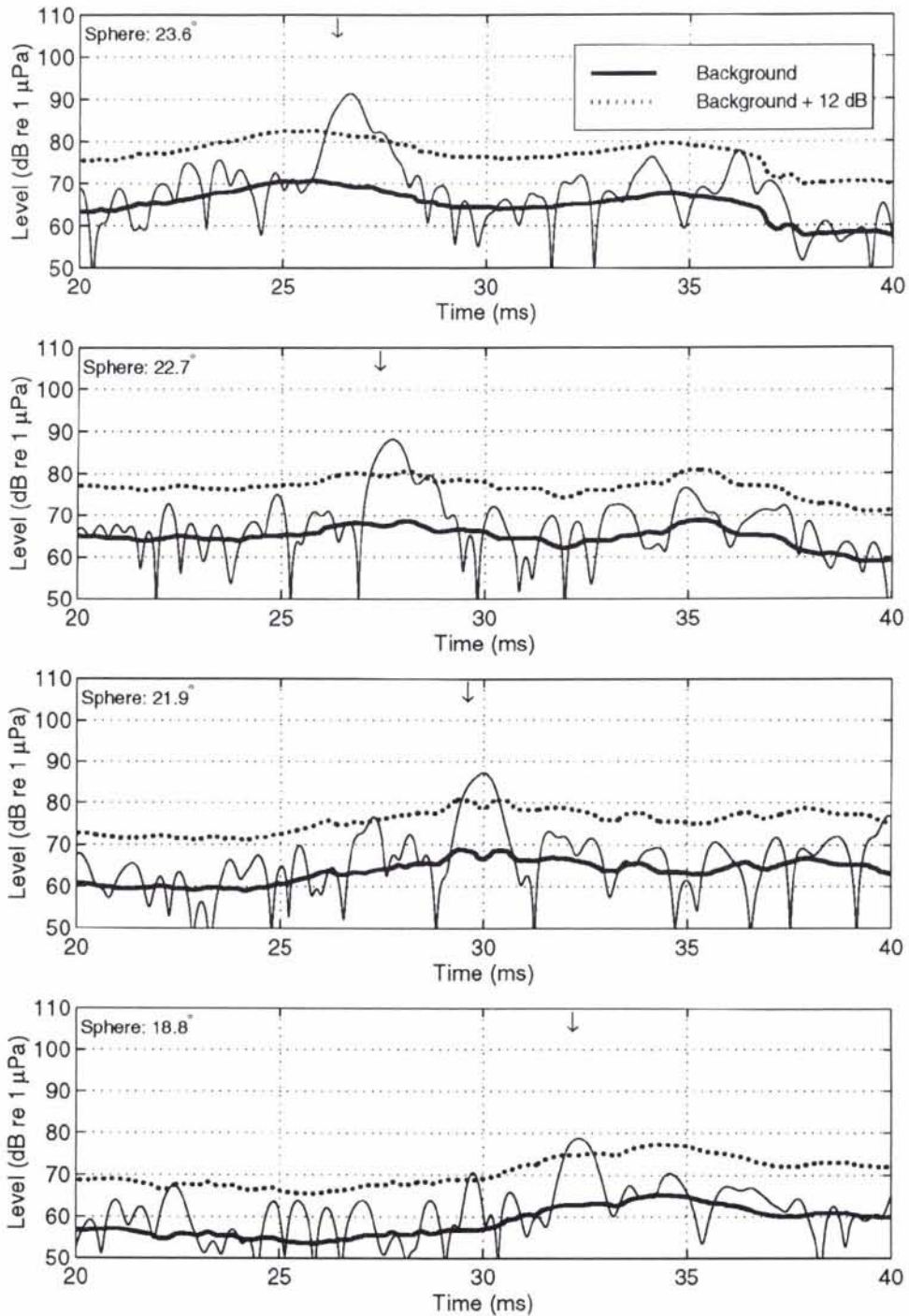


Figure 19 Sphere returns (lowpass filtered at 3 kHz) for four lowest grazing angles with background estimate.

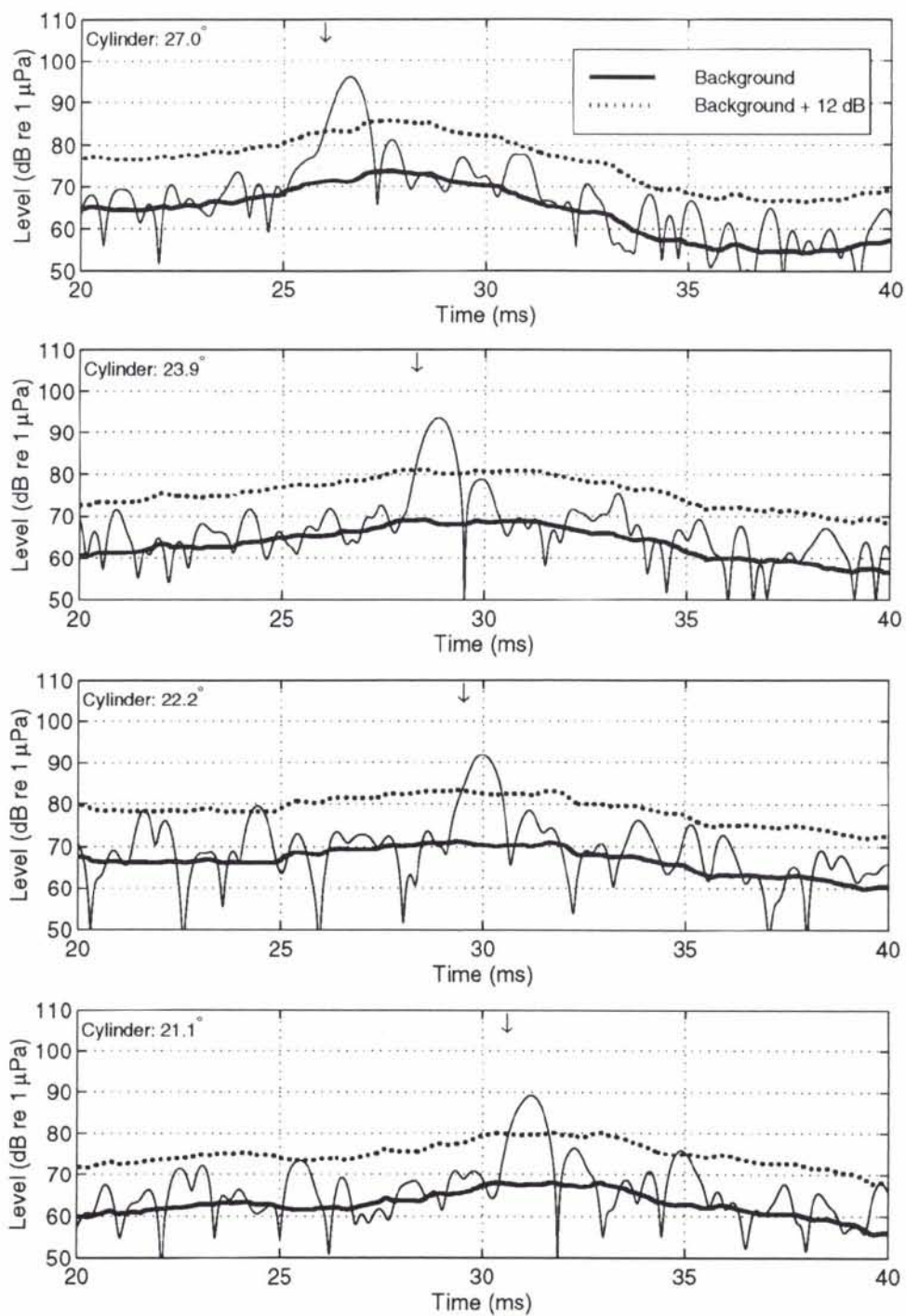


Figure 20 Cylinder returns (lowpass filtered at 3 kHz) for four highest grazing angles with background estimate.

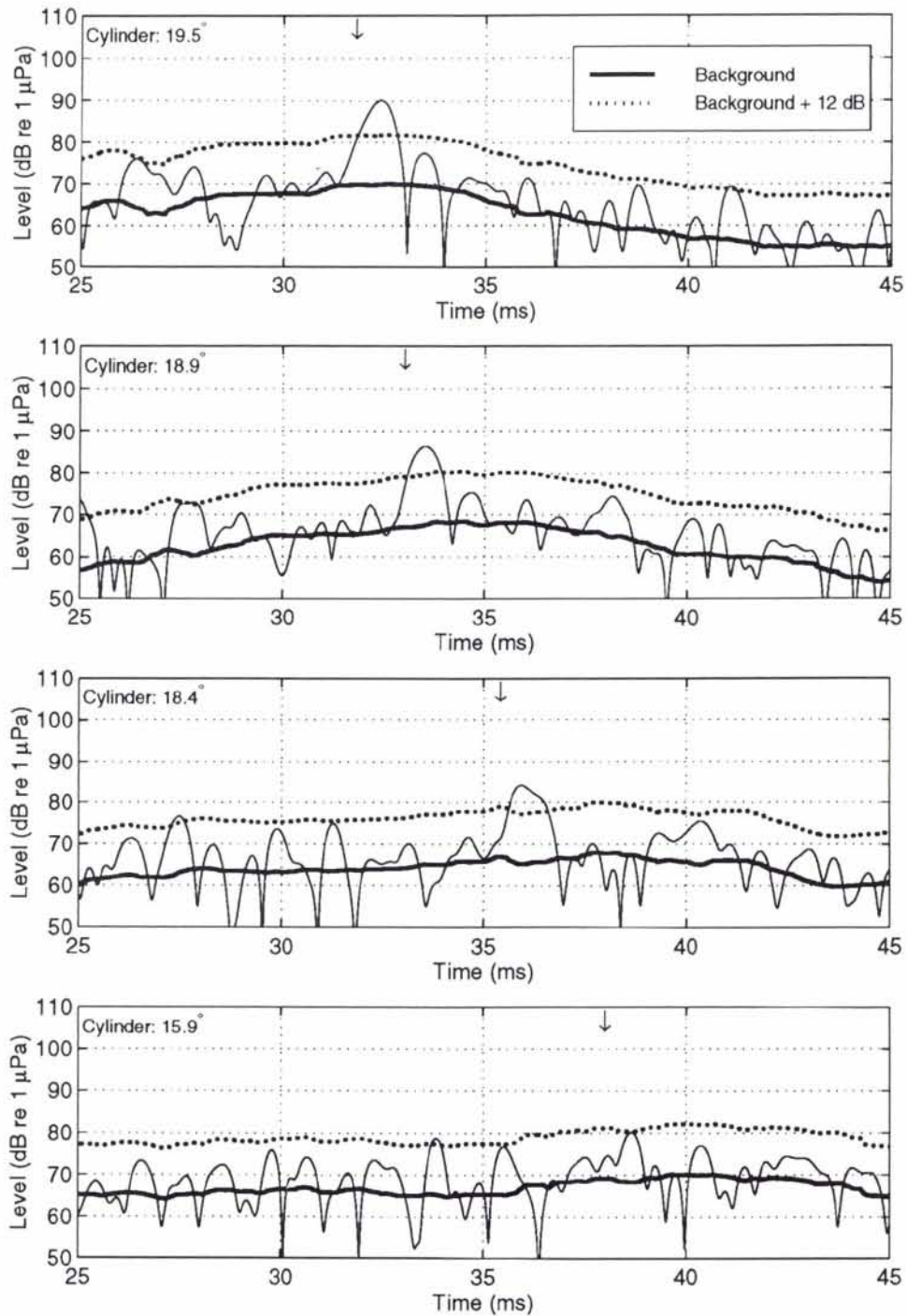


Figure 21 Cylinder returns (lowpass filtered at 3 kHz) for four lowest grazing angles with background estimate.

4.6 Full band – low frequency comparison

From the results shown in the previous subsection, SNR estimates can be made for each case by comparing the peaks of the target echoes to the background estimates as summarized in Fig. 22 for both the sphere (top) and the cylinder (bottom). Although the sand layer was very deep for this experimental site, meaning that sediment volume scattering should not play a large role, good “reverberation-only” measurements are not available. This does not allow, therefore, meaningful quantitative prediction of the expected results, hence more qualitative comments are warranted regarding the estimated SNR at this point.

For the sphere, markedly different results can be seen for the filtering operation as a function of grazing angle. For supercritical cases ($\theta_g > \theta_c \cong 27.6^\circ$), a reduction in SNR is seen with the lowpass filter. Figure 3 shows that for supercritical insonification the sphere response should be relatively frequency independent for $f > 3$ kHz. If the reverberation is also relatively frequency independent, this loss of SNR with reduction of the effective bandwidth is an expected result [5, 37]. If the reverberation falls off at lower frequencies, the reduction in effective bandwidth should be offset to some extent by the effect of emphasizing frequency bands where the signal level remains high but the noise is lower. The falloff in SNR seen in this analysis, however, indicates that there is most likely not a strong frequency dependence to the reverberation spectrum.

At lower grazing angles, some gain in SNR is achieved with the filtering operation. In this case, Fig. 3 shows the modeled decrease in the target response with increasing frequency. The filtering operation can be seen as maintaining target echo energy and rejecting reverberation energy for the subcritical cases.

The highest grazing angles measured with the sphere were not possible with the cylinder due to the geometry of the experiment. However, similar results can be seen with gains in SNR below the nominal critical angle when the filter is applied.

Another issue to keep in mind here is that the size of the insonified “patch” on the bottom contributing to reverberation is frequency dependent due to a $f^{-1/2}$ dependence of the transmit beamwidth [26]. Therefore, any gains in SNR are coming in spite of this reduced spatial resolution at the lower frequencies.

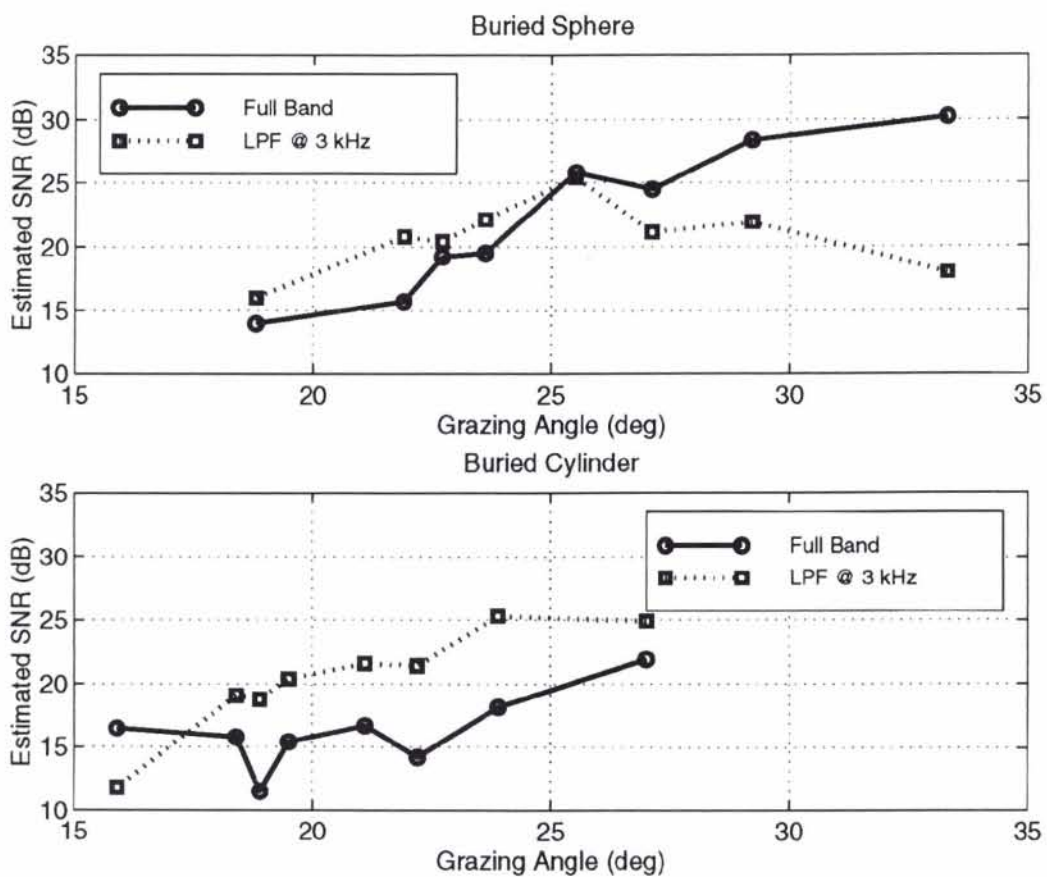


Figure 22 Summary of estimated SNR for sphere (top) and cylinder (bottom): full band and lowpass filtered results vs. grazing angle.

5

Discussion

This report has addressed the issue of acoustically detecting objects buried in ocean sediments at low grazing angles, i.e., beyond critical angle, in order to increase the coverage rate over system concepts that are designed to work within critical angle. Introductory material covered basic theoretical and modeling considerations. For penetration of acoustic energy into sandy seafloors with subcritical grazing angles, classical theory predicts that the evanescent component travelling parallel to the water-sand interface will coherently insonify buried targets with greater intensity at lower frequencies and shallower depths into the sediment. Some simulation results were covered which, in accordance with the evanescent wave theory for subcritical insonification, predict higher monostatic echo levels from buried objects at lower frequency. Also, recent work on modeling and measurement of reverberation due to bottom backscatter was reviewed, with special attention to the frequency dependence in the range of frequencies of interest for this work, i.e., 1–10 kHz. Although it is evident that BBS is highly dependent on the particular bottom under consideration, some general trends are worth noting. Regarding rough surface scattering alone, there is some evidence for lower BBS at lower frequencies. When the structure of the underlying seabed lends itself to producing sediment volume scattering, the effect is more noticeable at lower frequencies due to the increased acoustic penetration. Therefore, sediment volume scattering tends to “fill in” the BBS spectrum at lower frequencies for certain types of seabeds.

The main thrust of the report was then in describing a recent experiment designed to explore the characteristics of echoes from buried targets over a large relative bandwidth (~ 2 –16 kHz) and for grazing angles both above and below critical. Preliminary data analysis efforts have shown gains in SNR for subcritical insonification by considering only the lower part of the frequency band where the target echo is strongest. These results have at least partially verified the ideas behind the modeling work that has appeared previously, and is the first time, to the authors' knowledge, that this type of experimental data has been presented.

A great number of issues are still in need of attention, however, in order to fully address the design problem for higher coverage rate buried object detection sonars. It appears that many of the tools needed to do this work are now becoming available. *Validated* propagation, target scattering, and reverberation models are of key importance here, since when all the basic physical interactions are understood and can

be modeled, general system design approaches can be taken. More detailed model validation activities will be the next step in analyzing this data set and others like it to be collected in the near future.

Some interesting topics worthy of consideration are discussed below. One is the multipath nature of the target backscattering, as shown by the surface return in the beginning of Sect. 4. It makes intuitive sense to use as much of the energy scattered by the target as possible in a detection scheme, but issues related to fluctuation of the multipath returns due to surface movement and echo ambiguity if a low frequency vertical aperture is not practical should be addressed. In this same vein, multistatic geometries are currently being considered in order to sample the three-dimensional scattered field.

Also interesting is the topic of transmit signal and receiving filter design. As mentioned previously, optimal schemes can be devised given perfect knowledge of the noise and target echo. In the case of additive white Gaussian noise, the optimal receiving filter would be matched to the target echo (colored Gaussian noise can be dealt with through prewhitening). The lowpass filter employed in this preliminary analysis is then suboptimal, although it captures some of the flavor of the lowpass nature of the target echo. In any case, the gains seen in SNR give some level of confidence that robust processing methods can be devised that make minimal assumptions regarding target echo structure and noise characteristics.

It is worthwhile to note that the peak in the target echo level in Fig. 3 occurs near 1 kHz, at which frequency the sonar being used in this experiment has very low source levels. In order to more fully explore the lower frequency regimes of buried target scattering and bottom backscattering, SACLANTCEN is preparing to use a new parametric sonar with 15 kHz primary frequency and ~ 0.5 –5 kHz secondaries.

Further gains in coverage rate and SNR should also be possible through transmit and receive beamwidth design. Wider transmit beams cover larger portions on the seafloor for a given insonification, and horizontal apertures (physical or synthetic) provide better spatial resolution to limit reverberation.

Ultimately, system design work will depend on a series of trade-offs involving performance level (in terms of probabilities of detection and false alarm), coverage rate, hardware and processing complexity, etc.. The immediate goals of the continuation of this work are to be able to understand and quantify the basic physical interactions taking place so that the trade-offs mentioned above can be considered in a consistent and comprehensive way.

6

Acknowledgements

The experiment described in this report was a non-trivial exercise in the deployment of oceanic research equipment. Many thanks go to P. A. Sletner who served as Engineering Coordinator for the trial, and who contributed greatly to its overall success. We are also, once again, deeply in debt to the crew of T. B. Manning (A. Spairani, G. Bertoli, and G. Ciuffardi) for their expert handling of the vessel and experimental equipment. The electronics and data collection systems were professionally managed by A. Figoli, R. Chiarabini, and M. Mazzi. Diving tasks were essential to the experiment, and thanks go to M. Paoli, J. Staveley, and the team from Elba Yacht Assistance for their enthusiasm and efficiency. In addition, O. Bergem designed and programmed the original version of the data acquisition software used during the trial, and R. Hollett wrote the beamforming software used to analyze the data.

The authors would like to especially thank H. Schmidt for fruitful discussions on the topic of this report, and for providing the modeling results shown in Fig. 3. They would also like to thank E. Bovio, A. Lyons, M. Pinto, and D. Abraham for their interest and input.

References

-
- [1] C. A. C. van Niekerk, "Burial of small objects on the bottom of the North Sea," Master's thesis, Delft University of Technology, 1993.
- [2] F. B. Jensen, W. A. Kuperman, M. B. Porter, and H. Schmidt, *Computational Ocean Acoustics*. New York: AIP Press, 1994.
- [3] L. M. Brekhovskikh, *Waves in Layered Media*. New York: Academic Press, second ed., 1980.
- [4] E. L. Hamilton, "Compressional-wave attenuation in marine sediments," *Geophysics*, vol. 37, pp. 620–46, Aug. 1972.
- [5] A. W. Rihaczek, *Principles of High-Resolution Radar*. New York: McGraw Hill, 1969.
- [6] B. P. Lathi, *Modern Digital and Analog Communication Systems*. New York: Holt, Rinehart and Winston, 1983.
- [7] A. Maguer, E. Bovio, W. L. J. Fox, E. Pouliquen, and H. Schmidt, "Mechanisms for subcritical penetration into a sandy bottom: Experimental and modeling results," SR-287, NATO SACLANT Undersea Research Centre, La Spezia, Italy, 1998.
- [8] E. Pouliquen, A. Lyons, and N. G. Pace, "Penetration of acoustic waves into sandy seafloors at low grazing angles: The Helmholtz-Kirchhoff approach," SR-290, NATO SACLANT Undersea Research Centre, La Spezia, Italy, 1998.
- [9] R. Lim, J. L. Lopes, R. H. Hackman, and D. G. Todoroff, "Scattering by objects buried in underwater sediments: Theory and experiment," *Journal of the Acoustical Society of America*, vol. 93, pp. 1762–83, Apr. (Pt. 1) 1993.
- [10] H. T. Tamašauskas and J. A. Fawcett, "Scattering by spheres buried in sediment," SM-324, NATO SACLANT Undersea Research Centre, La Spezia, Italy, Jan. 1997.
- [11] J. A. Fawcett, "Scattering from an elastic cylinder buried beneath a rough water/sediment interface," in *High Frequency Acoustics in Shallow Water* (N. G. Pace, E. Pouliquen, O. Bergem, and A. P. Lyons, eds.), no. CP-45 in SACLANTCEN Conference Proceedings Series, pp. 147–54, NATO SACLANT Undersea Research Centre, June 1997.

- [12] J. A. Fawcett, "Modeling of scattering by partially buried elastic cylinders," SM-348, NATO SACLANT Undersea Research Centre, La Spezia, Italy, 1998.
- [13] P. H. Rogers, "Detection of buried mines using Rayleigh-scattered second-derivative Gaussian pulses," SR-235, NATO SACLANT Undersea Research Centre, La Spezia, Italy, Oct. 1995.
- [14] H. Schmidt, "Physics of 3-D scattering from rippled seabeds and buried targets in shallow water," SR-289, NATO SACLANT Undersea Research Centre, La Spezia, Italy, 1998.
- [15] H. Schmidt, "OASES: Version 2.1. User guide and reference manual," technical report, Massachusetts Institute of Technology, 1997.
- [16] H. Schmidt, J. Lee, H. Fan, and K. LePage, "Multistatic bottom reverberation in shallow water," in *High Frequency Acoustics in Shallow Water* (N. G. Pace, E. Pouliquen, O. Bergem, and A. P. Lyons, eds.), no. CP-45 in SACLANTCEN Conference Proceedings Series, pp. 475–81, NATO SACLANT Undersea Research Centre, June 1997.
- [17] R. J. Urick, *Principles of Underwater Sound*. New York: McGraw Hill, third ed., 1983.
- [18] Y. Y. Zhitovsky, "Sound backscattering by the ocean bottom (history and the state of the art)," *Acoustical Physics*, vol. 41, no. 5, pp. 686–90, 1995.
- [19] D. R. D. Balzo, J. H. Leclere, and M. J. Collins, "Critical angle and seabed scattering issues for active-sonar performance predictions in shallow water," in *High Frequency Acoustics in Shallow Water* (N. G. Pace, E. Pouliquen, O. Bergem, and A. P. Lyons, eds.), no. CP-45 in SACLANTCEN Conference Proceedings Series, pp. 123–30, NATO SACLANT Undersea Research Centre, June 1997.
- [20] J. W. Caruthers and J. C. Novarini, "A semi-empirical basis for a modified Lambert's law for low-grazing bottom backscattering," in *Oceans '95*, pp. 1676–83, IEEE, 1995.
- [21] P. D. Mourad and D. R. Jackson, "High frequency sonar equation models for bottom backscatter and forward loss," in *Oceans '89*, pp. 1168–75, IEEE, Jun. 1989.
- [22] P. D. Mourad and D. R. Jackson, "A model/data comparison for low-frequency bottom backscatter," *Journal of the Acoustical Society of America*, vol. 94, pp. 344–58, Jul. 1993.
- [23] A. P. Lyons, A. L. Anderson, and F. S. Dwan, "Acoustic scattering from the seafloor: Modeling and data comparison," *Journal of the Acoustical Society of America*, vol. 95, pp. 2441–51, Jul. (Pt. 1) 1994.

- [24] E. Pouliquen, O. Bergem, and N. G. Pace, "Time-evolution modelling of seafloor scatter. Part 1: Theory," SM-328, NATO SACLANT Undersea Research Centre, La Spezia, Italy, Apr. 1997.
- [25] Bentech Subsea AS, Stjørdal, Norway, *Simrad TOPAS PS 040 Operator Manual*.
- [26] T. G. Muir, "Nonlinear parametric transduction in underwater acoustics," in *1974 Ultrasonics Symposium Proceedings*, IEEE, 1974.
- [27] O. Bergem and N. G. Pace, "Calibration of the TOPAS PS040. Part I: Measurements recorded with TOPAS acquisition system," M-119, NATO SACLANT Undersea Research Centre, La Spezia, Italy, Jan. 1996.
- [28] E. A. Robinson and S. Treitel, *Geophysical Signal Analysis*. Englewood Cliffs, N.J.: Prentice-Hall, 1980.
- [29] S. Fioravanti, A. Maguer, W. L. J. Fox, L. Gualdesi, and A. Tesei, "Underwater rail facility for highly controlled experiments at sea." Submitted to Third European MAST Conference, Lisbon, Portugal, 1998.
- [30] J. A. Fawcett, W. L. J. Fox, and A. Maguer, "Modelling of scattering by objects on the seabed," SR-276, NATO SACLANT Undersea Research Centre, La Spezia, Italy, Oct. 1997.
- [31] W. L. J. Fox, J. A. Fawcett, D. Jourdain-Albonico, and A. Tesei, "Measurements of free-field acoustic scattering from cylindrical shells," SM-331, NATO SACLANT Undersea Research Centre, La Spezia, Italy, May 1997.
- [32] D. H. Johnson and D. E. Dudgeon, *Array Signal Processing: Concepts and Techniques*. Englewood Cliffs, N.J.: Prentice-Hall, 1993.
- [33] J. M. Hovem, "Detection of buried objects in the seabed," submitted for publication, NATO SACLANT Undersea Research Centre, La Spezia, Italy, 1997.
- [34] W. A. Struzinski and E. D. Lowe, "A performance comparison of four noise background normalization schemes proposed for signal detections systems," *Journal of the Acoustical Society of America*, vol. 76, pp. 1738–42, Dec. 1984.
- [35] P. P. Gandhi and S. A. Kassam, "Analysis of CFAR processors in nonhomogeneous background," *IEEE Transactions on Aerospace and Electronic Systems*, vol. 24, pp. 427–45, July 1988.
- [36] D. A. Abraham, "Modeling non-Rayleigh reverberation," SR-266, NATO SACLANT Undersea Research Centre, La Spezia, Italy, May 1997.
- [37] H. L. Van Trees, *Detection, Estimation, and Modulation Theory, Part III*. New York: Wiley, 1971.

Document Data Sheet

| | | |
|---|-----------------------------------|---|
| <i>Security Classification</i> | | <i>Project No.</i> 031-1 |
| <i>Document Serial No.</i> SR-293 | <i>Date of Issue</i> June 1998 | <i>Total Pages</i> 47 pp. |
| <i>Author(s)</i> Fox, W.L.J. and Maguer, A. | | |
| <i>Title</i> Detection of buried objects at low grazing angles: preliminary experimental results. | | |
| <i>Abstract</i> <p>The report considers the acoustic detection of objects buried in the seabed, and especially the possibility of using subcritical insonification geometries in order to increase coverage rate. Experimental results are presented for acoustic transmissions in the approximate frequency range 2–16 kHz both above and below the nominal critical angle of the sediment. The buried objects studied are a solid aluminium sphere of radius $a_s = 0.3$ m and a 2 m long water-filled cylindrical steel shell with radius $a_c = 0.25$ m. Preliminary processing of the data has shown that gains in signal-to-noise ratio can be obtained for subcritical cases by emphasizing the lower frequency components (in this case, $f < 3$ kHz) where models predict that the target echo is strongest due to the evanescent nature of the incident acoustic wave.</p> | | |
| <i>Keywords</i> Detection – buried – subcritical | | |
| <i>Issuing Organization</i> North Atlantic Treaty Organization SACLANT Undersea Research Centre Viale San Bartolomeo 400, 19138 La Spezia, Italy [From N. America: SACLANTCEN (New York) APO AE 09613] | | Tel: +39 0187 527 361 Fax: +39 0187 524 600 E-mail: library@saclantc.nato.int |

Initial Distribution for Unclassified SR-293

| <i>Ministries of Defence</i> | | <i>Scientific Committee of National Representatives</i> | |
|-----------------------------------|----|---|-----|
| DND Canada | 10 | SCNR Belgium | 1 |
| CHOD Denmark | 8 | SCNR Canada | 1 |
| DGA France | 8 | SCNR Denmark | 1 |
| MOD Germany | 15 | SCNR Germany | 1 |
| HNDGS Greece | 12 | SCNR Greece | 1 |
| MARISTAT Italy | 9 | SCNR Italy | 1 |
| MOD (Navy) Netherlands | 12 | SCNR Netherlands | 2 |
| NDRE Norway | 10 | SCNR Norway | 1 |
| MOD Portugal | 5 | SCNR Portugal | 1 |
| MDN Spain | 2 | SCNR Spain | 1 |
| TDKK and DNHO Turkey | 5 | SCNR Turkey | 1 |
| MOD UK | 20 | SCNR UK | 1 |
| ONR USA | 34 | SCNR USA | 2 |
| | | French Delegate | 1 |
| | | SECGEN Rep. SCNR | 1 |
| | | NAMILCOM Rep. SCNR | 1 |
| <i>NATO Commands and Agencies</i> | | | |
| NAMILCOM | 2 | | |
| SACLANT | 3 | <i>National Liaison Officers</i> | |
| CINCEASTLANT/ | | NLO Canada | 1 |
| COMNAVNORTHWEST | 1 | NLO Denmark | 1 |
| CINCIBERLANT | 1 | NLO Germany | 1 |
| CINCWESTLANT | 1 | NLO Italy | 1 |
| COMASWSTRIKFOR | 1 | NLO Netherlands | 1 |
| COMMAIREASTLANT | 1 | NLO Spain | 1 |
| COMSTRIKFLTANT | 1 | NLO UK | 1 |
| COMSUBACLANT | 1 | NLO USA | 1 |
| SACLANTREPEUR | 1 | | |
| SACEUR | 2 | | |
| CINCNORTHWEST | 1 | | |
| CINC SOUTH | 1 | | |
| COMEDCENT | 1 | | |
| COMMARAIRMED | 1 | | |
| COMNAVSOUTH | 1 | Sub-total | 200 |
| COMSTRIKFOR SOUTH | 1 | | |
| COMSUBMED | 1 | SACLANTCEN | 30 |
| NC3A | 1 | | |
| PAT | 1 | Total | 230 |